cmgh
CELLULAR AND MOLECULAR GASTROENTEROLOGY AND HEPATOLOGY

ORIGINAL RESEARCH

Inhibition of EZH2 Reduces Aging-Related Decline in Interstitial Cells of Cajal of the Mouse Stomach

Negar Taheri,[1,2] Egan L. Choi,[1,2] Vy Truong Thuy Nguyen,[1,2] Yuebo Zhang,[1,2] Nick M. Huynh,[1,2] Todd A. Kellogg,[3] Andre J. van Wijnen,[4] Tamas Ordog,[1,2] and Yujiro Hayashi[1,2]

[1]Enteric Neuroscience Program and Department of Physiology and Biomedical Engineering, Mayo Clinic College of Medicine and Science, Rochester, Minnesota; [2]Gastroenterology Research Unit, Division of Gastroenterology and Hepatology, Department of Medicine, Mayo Clinic College of Medicine and Science, Rochester, Minnesota; [3]Department of Surgery, Mayo Clinic College of Medicine and Science, Rochester, Minnesota; and [4]Department of Biochemistry, University of Vermont, Burlington, Vermont

SUMMARY

Depletion of interstitial cells of Cajal contributes to aging-associated restriction of gastric functions and consequent reduced food intake. The polycomb histone methyltransferase EZH2 is central to ICC loss. EZH2 inhibition prevents this change and preserves gastric functions and food intake.

BACKGROUND & AIMS: Restricted gastric motor functions contribute to aging-associated undernutrition, sarcopenia, and frailty. We previously identified a decline in interstitial cells of Cajal (ICC; gastrointestinal pacemaker and neuromodulator cells) and their stem cells (ICC-SC) as a key factor of gastric aging. Altered functionality of the histone methyltransferase enhancer of *zeste* homolog 2 (EZH2) is central to organismal aging. Here, we investigated the role of EZH2 in the aging-related loss of ICC/ICC-SC.

METHODS: *klotho* mice, a model of accelerated aging, were treated with the most clinically advanced EZH2 inhibitor, EPZ6438 (tazemetostat; 160 mg/kg intraperitoneally twice a day for 3 weeks). Gastric ICC were analyzed by Western blotting and immunohistochemistry. ICC and ICC-SC were quantified by flow cytometry. Gastric slow wave activity was assessed by intracellular electrophysiology. *Ezh2* was deactivated in ICC by treating $Kit^{creERT2/+}$;$Ezh2^{fl/fl}$ mice with tamoxifen. TRP53, a key mediator of aging-related ICC loss, was induced with nutlin 3a in gastric muscle organotypic cultures and an ICC-SC line.

RESULTS: In *klotho* mice, EPZ6438 treatment mitigated the decline in the ICC growth factor KIT ligand/stem cell factor and gastric ICC. EPZ6438 also improved gastric slow wave activity and mitigated the reduced food intake and impaired body weight gain characteristic of this strain. Conditional genomic deletion of *Ezh2* in *Kit*-expressing cells also prevented ICC loss. In organotypic cultures and ICC-SC, EZH2 inhibition prevented the aging-like effects of TRP53 stabilization on ICC/ICC-SC.

CONCLUSIONS: Inhibition of EZH2 with EPZ6438 mitigates aging-related ICC/ICC-SC loss and gastric motor dysfunction, improving slow wave activity and food intake in *klotho* mice.

(Cell Mol Gastroenterol Hepatol 2024;18:101376; https://doi.org/10.1016/j.jcmgh.2024.101376)

Keywords: klotho; $Kit^{creERT2/+}$; $Ezh2^{fl/fl}$; Gastric Motility; Food Intake.

The population of individuals aged 60 years and older is experiencing exponential growth. It is projected that the proportion of this demographic will nearly double from 12% to 22% by 2050. Although aging itself does not directly cause diseases and disorders, age-related biologic defects (eg, stem cell depletion, DNA damage) are prominent contributors and age is a risk factor for numerous diseases and disorders, imposing a substantial health care burden.[1–4] Consequently, all countries will inevitably encounter significant challenges in addressing the ailments and conditions afflicting the geriatric population. In general, the process of aging leads to a gradual decline in the functionality of most organs and tissues, including the stomach.[2] Among the gastric symptoms associated with aging are early fullness, nausea, abdominal pain, and indigestion. Although these symptoms may be relatively mild, they contribute to subsequent reductions in food intake, undernutrition, and unfavorable health outcomes, such as sarcopenia and frailty.[5–7] This phenomenon is often referred

Abbreviations used in this paper: **AF, alexa fluor; ANO1, anoctamin 1; Cy5, cyanine 5; Cy7, cyanine 7; DAPI, 4',6-diamidino-2-phenylindole; ERK, extracellular signaling-regulated kinase; EZH2, enhancer of zeste homolog 2; H3K27me3, trimethylation of lysine 27 of histone 3; ICC, interstitial cells of Cajal; ICC-SC, interstitial cell of Cajal stem cells; IGF1, insulin-like growth factor 1; KIT, v-kit Hardy-Zuckerman 4 feline sarcoma viral oncogene homolog; MDM2, murine double minute 2; MTS, methyltetrazolium salt; PE, phycoerythrin; PRC, polycomb repressive complex(es); P-TRP53, TRP53 phosphorylation; SCF, stem cell factor; Scr, scrambled sequences; siRNA, small interfering RNA; TRP53, transformation related protein 53; tsTAg, tsA58-mutant SV40 large T antigen; T-TRP53, total TRP53; WB, Western immunoblotting; WT, wild-type.**

Most current article

2352-345X
https://doi.org/10.1016/j.jcmgh.2024.101376

to as "anorexia of aging."[8] Hence, gaining a deeper understanding of age-related gastric dysfunctions is crucial for the development of effective treatments aimed at preventing or reversing these conditions.

Regulation of gastric motility is a complex process involving multiple components. Smooth muscle cells are responsible for executing mechanical work, whereas enteric neurons establish reflexes and control functions, such as accommodation and sphincter activity.[9,10] Additionally, interstitial cells of Cajal (ICC), mesenchymal cells in the gut, play a crucial role by generating propagating electrical slow wave activity, which underlies the rhythmic contractions of smooth muscles, mediating nitrergic and cholinergic neuromuscular neurotransmission, and by setting resting membrane potential and muscle tone.[9,10] In previous studies, we observed a significant decline in ICC and ICC stem/progenitor cells (ICC-SC) in the stomachs of naturally aged mice and *klotho* mice, a model of accelerated aging,[11] which occurred without a corresponding loss of enteric neurons or smooth muscle cells.[12] This age-related loss of ICC was accompanied by impaired relaxation of the fundus and reduced gastric compliance. These changes paralleled diminished food intake and impaired body weight gain in *klotho* mice.[12]

Recently, we reported the intriguing finding that activation of the extracellular signaling-regulated kinase (ERK) 1/2 (mitogen-activated protein kinase 3 and 1) pathway by insulin-like growth factor 1 (IGF1) mitigates loss of ICC and ICC-SC.[13] Furthermore, activation of the IGF1-ERK1/2 axis improves gastric compliance, food intake, and body weight in *klotho* mice.[13] Interestingly, a recent study demonstrated that IGF1 enhanced the accessibility of chromatin in hematopoietic stem cells, leading to the rejuvenation of their impaired functions.[14] Although our previous study also demonstrated the beneficial effects of IGF1 on ICC-SC aging, the specific epigenetic alterations occurring in ICC-SC/ICC during the aging process remain unclear and warrant further investigation.

One crucial mechanism that has been proposed to contribute to the aging of stem cells and organismal aging is altered functionality of polycomb repressive complexes (PRC) 1 and 2.[15,16] These complexes typically repress the transcriptional program that inhibits cell cycle progression, allowing for self-renewal to persist.[17] Of particular significance in this context is the histone methyltransferase enhancer of *zeste* homolog 2 (EZH2), which is a key component of PRC2.[16,17] EZH2 is responsible for trimethylation of lysine 27 of histone 3 (H3K27me3) during development, and in various diseases and conditions.[15,17] In aged cells and tissues, studies have demonstrated that EZH2 disassociates from the promoter region of the cyclin-dependent kinase inhibitor *Cdkn2a* encoding *INK4A* and *ARF*,[18] ultimately leading to cell cycle arrest.[18] Although DNA occupancy by H3K27me3 generally decreases with aging,[19] increased EZH2-mediated repression has been shown in specific cell types including muscle and mesenchymal cells.[20] However the role of EZH2 in the aging of gastric ICC-SC/ICC remains unknown. Therefore, we studied the effects of pharmacologic and genetic manipulation of EZH2 on ICC and ICC-SC and their functions in *klotho* mice and in mice with Ezh2 deletion in ICC in vivo and ex vivo, and in cultured ICC-SC and gastric organotypic cultures ex vivo. Our results indicate a role for increased EZH2-mediated H3K27 trimethylation in aging-related repression of KIT and stem cell factor (SCF) levels, depletion of gastric ICC, and consequent decline in gastric motor function, food intake, and body weight gain, highlighting a potential avenue for pharmacologic interventions to prevent frailty.

Results

EZH2 and H3K27me3 Are Upregulated and KIT and ANO1 Are Reduced in Aging Gastric Muscles of Mice and Humans

Reduced EZH2 protein may contribute to the age-dependent decline in various stem cells and organ functions.[18,21] Based on previous reports, we hypothesized that EZH2 expression would decrease with age leading to ICC-SC decline and aging-related gastric motor dysfunction. First we measured gastric EZH2 protein and H3K27me3 levels and ICC markers in naturally aged mice (C57BL/6J background) and *klotho* mice (C3H background), a model of accelerated aging.[11] We unexpectedly found that EZH2 protein and H3K27me3 levels were elevated in gastric muscles of old mice (22–24 months old, which is equivalent to ∼70-year-old humans)[22] and *klotho* mice versus age-matched wild-type (WT) mice (60–70 days old, which is biologically equivalent to human adolescence) (Figure 1*A* and *B*). Consistent with our previous research and other data,[23] we also detected a significant reduction in both v-kit Hardy-Zuckerman 4 feline sarcoma viral oncogene homolog (KIT, a receptor for SCF and a key ICC developmental and survival factor) and anoctamin 1 (ANO1; a calcium-activated chloride channel important for ICC functions) protein in the stomachs of old and *klotho* mice (Figure 1*A* and *B*). It is important to note that there were no significant differences observed between males and females in naturally aged and *klotho* mice (Figure 1*A* and *B*). To relate mouse findings to human subjects, we also measured gastric EZH2 and H3K27me3 levels and ICC markers in gastric tunica muscularis tissues from male and female patients aged 28–68 years. Gastric EZH2 protein and H3K27me3 levels gradually increased with age, and this increase was inversely associated with the reduction of KIT and ANO1 in the stomachs of men (Figure 1*C*) and women (Figure 1*D*). These findings suggest that different mechanisms may be operative in the ICC lineage compared with other cell types.

Pharmacologic and RNA Interference-mediated Inhibition of Ezh2 Prevents the Cytostatic Effects of TRP53 Stabilization with Nutlin 3a in Cultured ICC-SC

We previously reported that transformation-related protein 53 (TRP53/p53) is a key mediator of age-related ICC-SC depletion.[24] In ICC-SC cultures (D2211B cell line) previously established by our group,[25] TRP53 upregulation with nutlin 3a, an inhibitor of the TRP53-degrading E3 ubiquitin ligase murine double minute 2 (MDM2), also

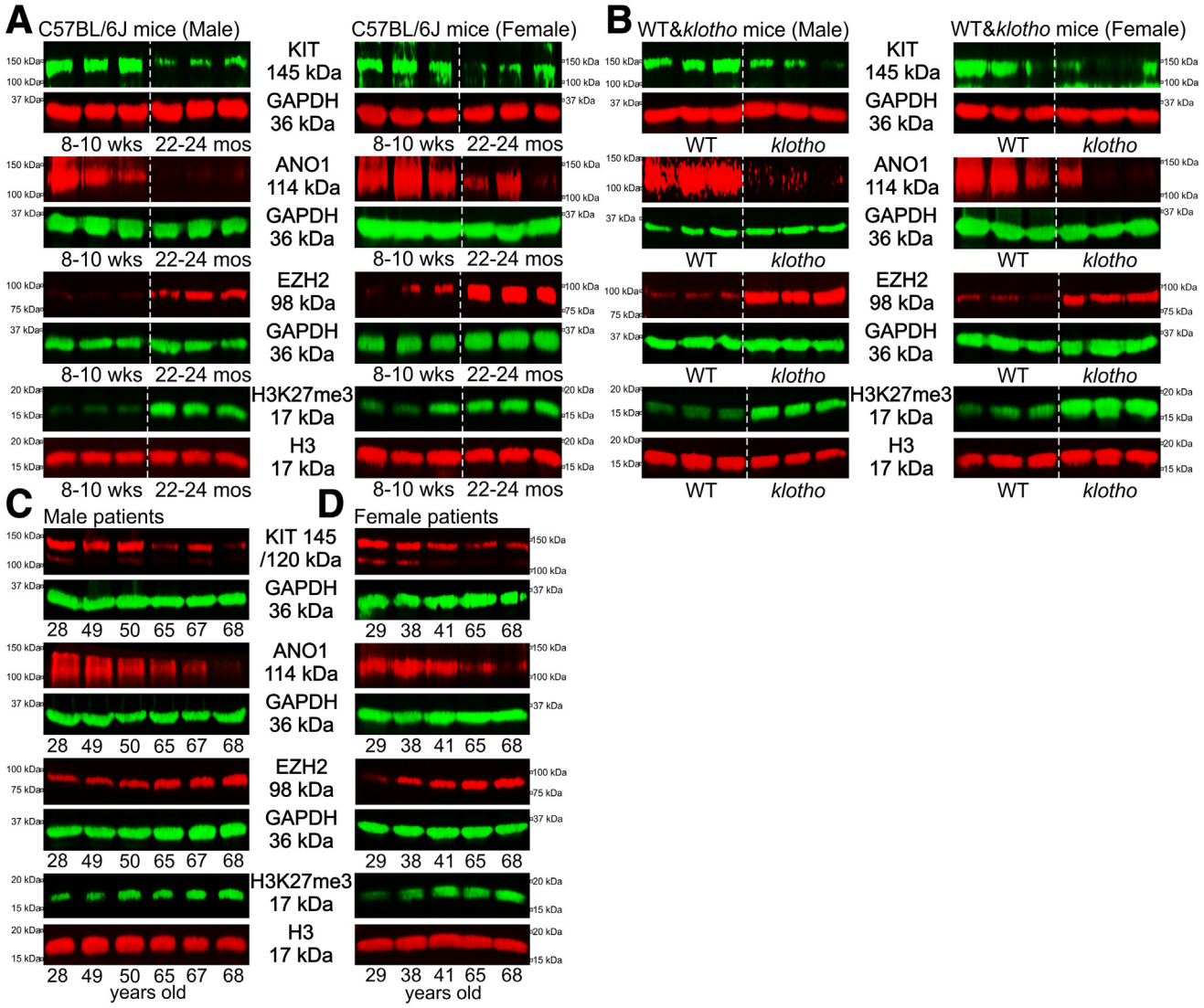

Figure 1. Upregulation of PRC2 regulates gastric tissue aging. (*A* and *B*) Downregulated ICC makers (KIT and ANO1 protein) and upregulated EZH2 protein and increased H3K27me3 levels in gastric tissues of *klotho* relative to WT mice and in old mice (22–24 months old) compared with young control animals (8–10 weeks old). The *klotho* and WT mice were used between 60 and 70 days of age. Glyceraldehyde-3-phosphate dehydrogenase (GAPDH) was used as a loading control. (*C* and *D*) Age-associated downregulation of KIT and ANO1 and upregulation of EZH2 protein and H3K27me3 levels in gastric muscles of patients between 28 and 68 years of age in (*C*) men and (*D*) women.

increased EZH2 protein and H3K27me3 levels without affecting TRP53 phosphorylation (P-TRP53) (Figure 2*A*). The 150-fold less potent enantiomer nutlin 3b was used as control for nutlin 3a. These findings suggest that TRP53 activation during aging is critical for EZH2-mediated histone methylation. Based on these observations, we hypothesized that EZH2 inhibition can prevent or delay TRP53-induced ICC-SC depletion. For this purpose, we used EPZ6438 (tazemetostat), an inhibitor of EZH2 catalytic function,[26,27] which has been approved by the Food and Drug Administration for the treatment of relapsed or refractory follicular lymphoma and epithelioid sarcoma. We found that 3-day treatment with 500 nmol/L EPZ6438[28] prevented TRP53-induced H3K27me3 upregulation by Western immunoblotting (WB) and cell growth arrest by methyltetrazolium salt (MTS) assay without affecting TRP53 and EZH2 protein expression (Figure 2*B*). Because *Kit* is known to be a target of PRC2-mediated epigenetic repression in embryonic fibroblasts,[17] we investigated if PRC2-mediated H3K27me3 contributes to the reduced expression of KIT protein induced by nutlin 3a. We found that EPZ6438 treatment significantly increased KIT protein expression in presence and absence of nutlin 3a. Although nutlin 3a did decrease KIT protein expression, this effect was not significant, likely because of the inherently low KIT expression in ICC-SC. We also detected similar effects on TRP53-induced ICC-SC aging using 500 nmol/L GSK126,[28] a second highly specific inhibitor of EZH2 (Figure 2*D*). These results indicate that pharmacologic EZH2 inhibition upregulates KIT and stimulates the proliferation of ICC-SC cell lines via H3K27me3

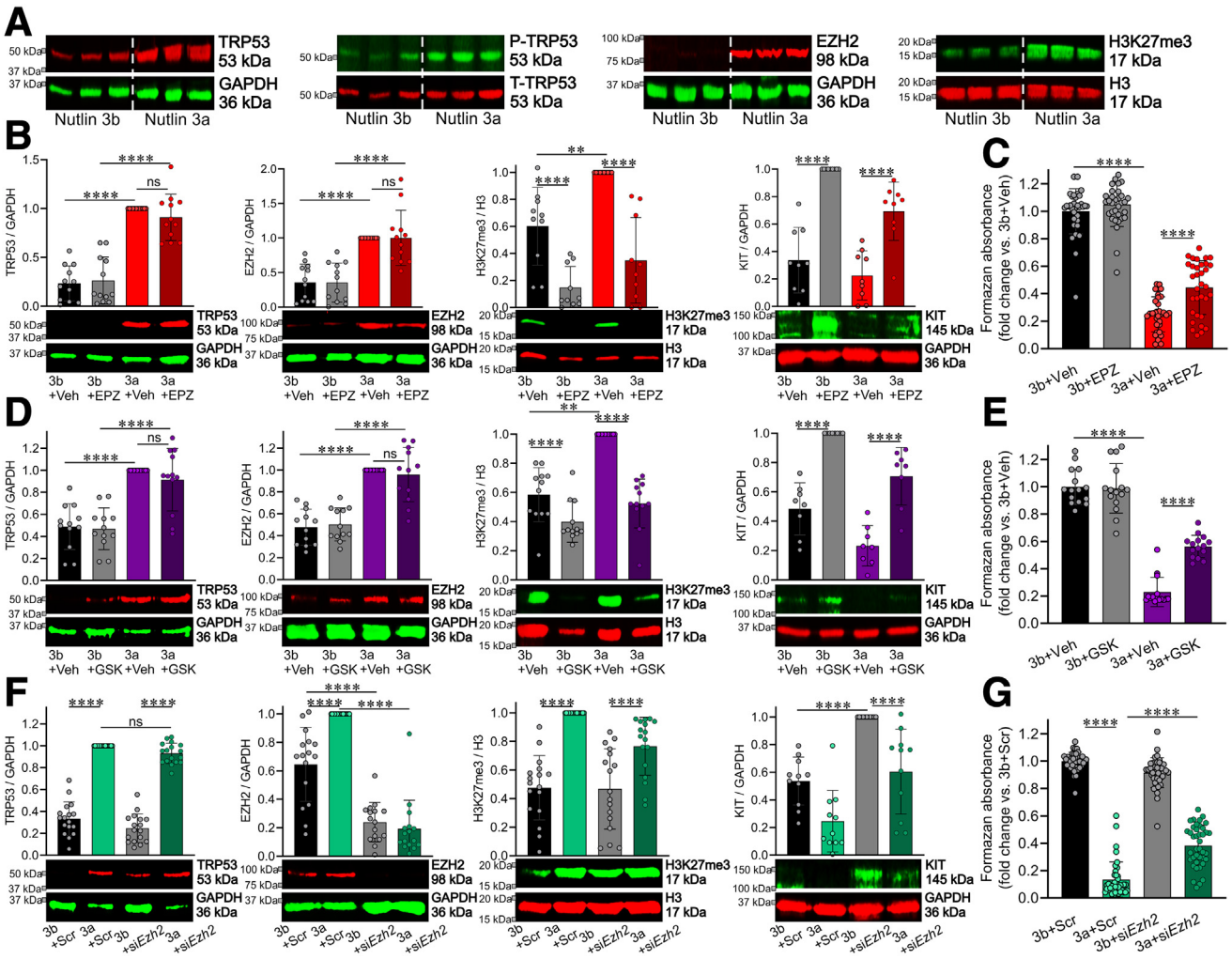

Figure 2. PRC2 regulates ICC-SC aging. *(A)* Activation of TRP53 by nutlin 3a (30 μmol/L, 72 hours) upregulated EZH2 protein and increased H3K27me3 levels in D2211B ICC-SC without affecting TRP53 phosphorylation (P-TRP53). The 150-fold less potent enantiomer nutlin 3b (30 μmol/L, 72 hours) used as control for nutlin 3a. *(B–E)* Ezh2 inhibitors (EPZ6438 [EPZ] and GSK126 [GSK]) applied at 500 nmol/L for 72 hours prevented nutlin 3a (30 μmol/L, 72 hours)-induced H3K27me3 (n = 8–9/group) and cell growth arrest (n = 15/group) without affecting TRP53 and EZH2 protein expression in ICC-SC (D2211B cells). The inactive enantiomer nutlin 3b (3b; 30 μmol/L) served as a control for nutlin 3a. *(F* and *G)* siRNA-mediated knockdown *Ezh2* (si*Ezh2*) prevented nutlin 3a-induced EZH2 upregulation (n = 9/group) and cell growth arrest (n = 30/group) without affecting TRP53 protein expression and H3K27me3 levels in ICC-SC (D2211B cells). Corresponding Scr served as a control for si*Ezh2*. Statistical significance was determined using Kruskal-Wallis 1-way analysis of variance (on ranks). *$P < .05$, **$P < .01$, ****$P < .0001$. ns, not significant.

inhibition. To obtain direct evidence of EZH2 involvement in TRP53-induced ICC-SC depletion, we performed small interfering RNA (siRNA)-mediated knock-down of EZH2 in ICC-SC. Scrambled sequences (Scr) were used as a control. EZH2 knockdown robustly downregulated EZH2 protein in ICC stem cells (Figure 2*F*) and attenuated nutlin 3a-induced EZH2 protein upregulation by WB and cell growth arrest by MTS assay (Figure 2*G*). These findings indicate that selective EZH2 inhibition mitigates TRP53-induced ICC-SC depletion.

Prevention of TRP53-induced and EZH2-mediated ICC Loss by EPZ6438

To translate our in vitro findings into more physiologically relevant contexts, we investigated the effects of pharmacologic EZH2 inhibition on TRP53-induced ICC depletion using organotypic cultures (ex vivo culture systems) of gastric corpus and antrum muscles. In our previous study, we observed that nutlin 3a increased TRP53 protein expression in a dose-dependent manner and decreased ICC in organotypic cultures.[13] In the current study, we confirmed that nutlin 3a at a concentration of 30 μmol/L upregulated TRP53 protein and reduced KIT protein by WB (Figure 3*A*, *top*). Consistent with findings in ICC-SC cultures, the same treatment also increased EZH2 protein and H3K27me3 (Figure 3*A*, *bottom*). Next, we investigated whether inhibiting EZH2 with EPZ6438 could mitigate the ICC loss induced by nutlin 3a. We found that a 3-day treatment with 500 nmol/L EPZ6438 prevented the

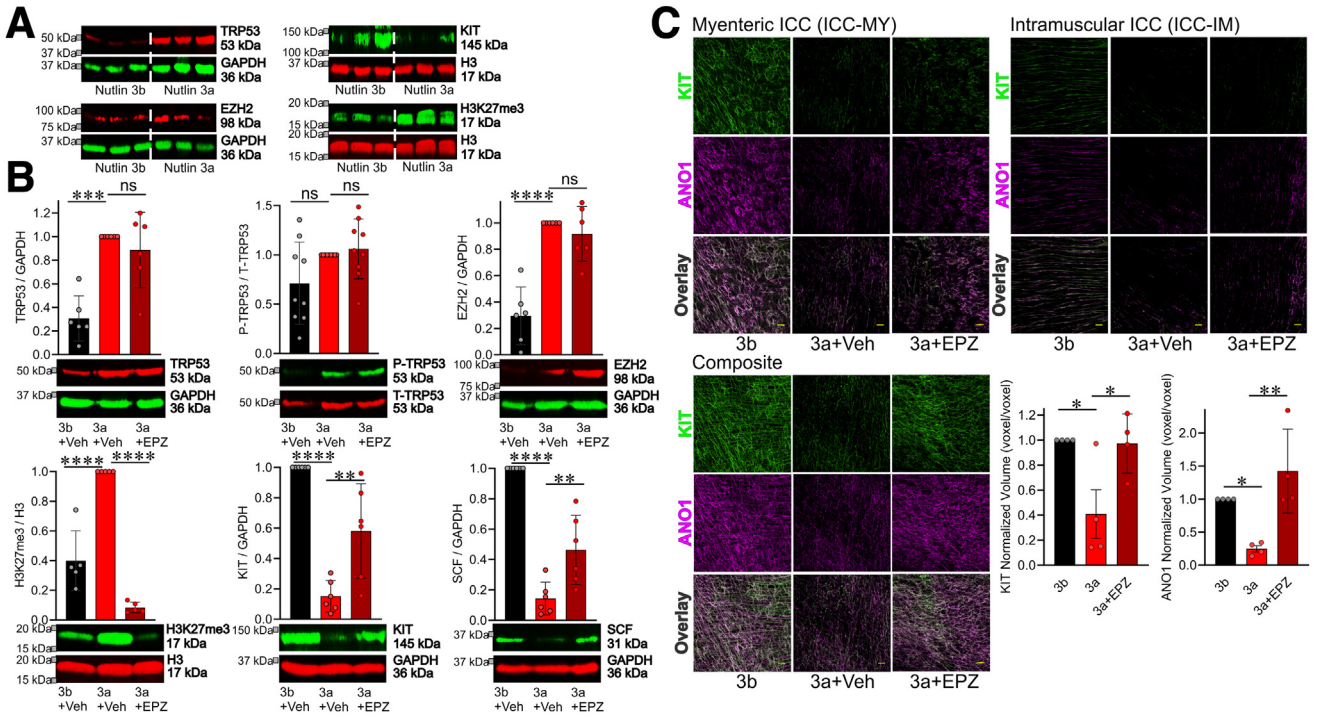

Figure 3. Inhibition of H3K27me3 by EPZ6438 mitigates TRP53-induced ICC loss. *(A)* Activation of TRP53 by nutlin 3a (30 μmol/L, 72 hours) downregulated KIT protein, upregulated EZH2 protein, and increased H3K27me3 levels in gastric organotypic cultures from stomachs of C57BL/6 mouse aged 12–14 days old. The 150-fold less potent enantiomer nutlin 3b (30 μmol/L, 72 hours) used as control for nutlin 3a. (*B*) EPZ6438 (500 nmol/L) mitigated nutlin 3a-induced (30 μmol/L) upregulated H3K27me3 levels (*lower left*), reduced KIT protein (*lower middle*), and reduced SCF protein (*lower right*) in gastric corpus + antrum tunica muscularis organotypic cultures from 12- to 14-day-old C57BL/6J mice (n = 6/group). EPZ6438 had no effect on nutlin 3a-induce upregulated TRP53 protein (*upper left*), TRP53 phosphorylation (*upper middle*) and upregulated EZH2 protein expression (*upper right*). The inactive enantiomer nutlin 3b (3b; 30 μmol/L) served as a control for nutlin 3a. Glyceraldehyde-3-phosphate dehydrogenase (GAPDH) was used as a loading control. Statistical significance was determined using Kruskal-Wallis 1-way analysis of variance (on ranks). (*C*) Reduced gastric ICC networks by nutlin 3a (30 μmol/L) in gastric corpus + antrum tunica muscularis organotypic cultures from 12- to 14-day-old C57BL/6J mice were restored by EPZ6438 (500 nmol/L) treatment. Representative confocal stacks showing KIT$^+$ (*green*) and ANO1$^+$ (*magenta*) myenteric ICC (ICC-MY) and intramuscular ICC (ICC-IM) in corresponding regions of the gastric corpus (greater curvature, full thickness) of nutlin 3b (3b; 30 μmol/L) + vehicle, nutlin 3a (30 μmol/L) + vehicle, and nutlin 3a (3a; 30 μmol/L) + EPZ6438 (EPZ; 500 nmol/L). n = 4 /group. Scale bar: 50 μm Statistical significance was determined using Kruskal–Wallis 1-way analysis of variance (on ranks). *P < .05, **P < .01, ***P < .001, ****P < .0001. ns, not significant.

TRP53-induced increase in H3K27me3 and decreased KIT protein levels without affecting TRP53 and EZH2 protein expression and TRP53 phosphorylation by WB (Figure 3*B*). To confirm the restoration of nutlin 3a-induced ICC depletion by EPZ6438 treatment, we conducted KIT and ANO1 coimmunostaining and quantified the volume of KIT or ANO1 immunofluorescence in the stomach using a Nikon GA3 recipe. Quantitative image analysis verified the recovery of ICC depletion induced by nutlin 3a following EPZ6438 treatment (Figure 3*C*). Overall, these findings suggest that TRP53 activation is important for EZH2-mediated histone methylation, leading to ICC depletion during aging. SCF is the natural ligand of KIT and critical for the differentiation, proliferation, migration, survival, and functional activation of ICC.[25,29–31] Previously, we found that EZH2 represses SCF expression by contributing to the maintenance of a repressive chromatin state of *Kitl* promoter.[32] We also found that SCF is reduced in *klotho* mice and IGF1 upregulated SCF protein expression via downregulation of H3K27me3 in organotypic cultures of juvenile BALB/c mouse stomachs.[32] In addition, we demonstrated that pharmacologic EZH2 inhibition by adenosine dialdehyde upregulates SCF protein expression in organotypic cultures.[32] Thus, we measured SCF protein expression. Nutlin 3a treatment reduced SCF protein expression, and this reduction was significantly mitigated by EPZ6438 treatment (Figure 3*B*, *lower right*), suggesting restoring SCF might contribute to the effect of EPZ6438 on ICC decline.

EPZ6438 Mitigates the Reduction of Gastric ICC during Aging

We next hypothesized that pharmacologic EZH2 inhibition can also mitigate the age-related decline in gastric ICC and improve gastric motor dysfunction, consequent reduced food intake, and impaired body weight gain in progeric *klotho* mice. To this end, *klotho* mice at 4–5 weeks of age were treated with EPZ6438 (160 mg/kg intraperitoneally

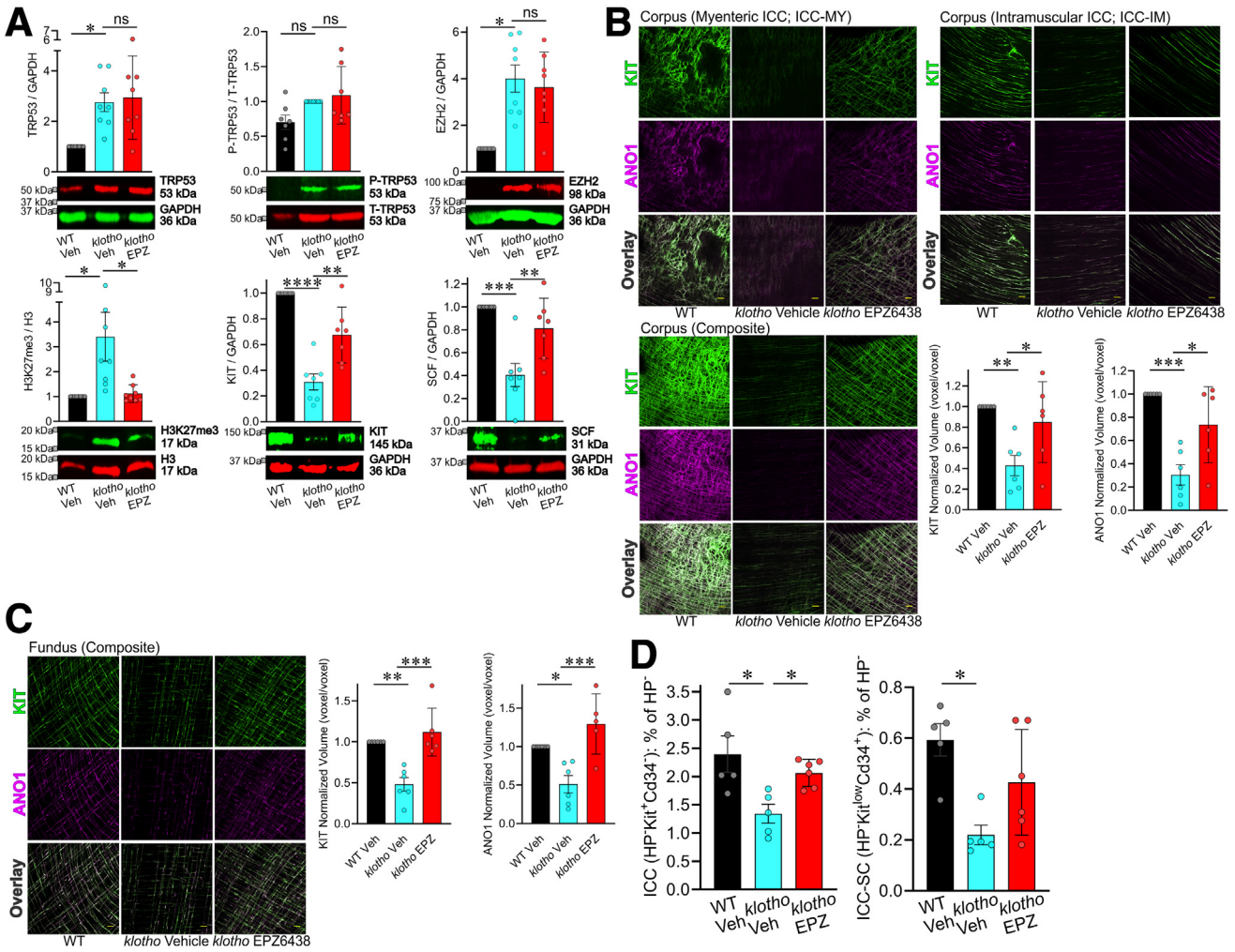

Figure 4. EPZ6438 treatment restored age-related ICC/ICC-SC decline via activation of the SCF-KIT pathway in *klotho* mice. (*A*) EPZ6438 (EPZ) restored upregulated H3K27me3 levels (*lower left*), reduced KIT protein (*lower middle*), and reduced SCF protein (*lower right*) in gastric tunica muscularis of *klotho* mice (n = 7/group). EPZ6438 had no effect on upregulated TRP53 protein (*upper left*), TRP53 phosphorylation (*upper middle*), and upregulated EZH2 protein expression (*upper right*). Vehicle (Veh) was used as a control for EPZ6438. Glyceraldehyde-3-phosphate dehydrogenase (GAPDH) was used as a loading control. (*B*) Reduced gastric ICC networks in *klotho* mice were restored by EPZ6438 treatment. Representative confocal stacks showing KIT$^+$ (*green*) and ANO1$^+$ (*magenta*) myenteric ICC (ICC-MY), and intramuscular ICC (ICC-IM) in corresponding regions of the gastric corpus (*B*; greater curvature, full thickness) and fundus (*C*; greater curvature, full thickness) of a WT and *klotho* mice. n = 5/group. Scale bar: 50 μm. (*D*) Normalized ICC (KIT$^+$CD34$^-$ cells) and ICC-SC (KIT^{low}CD34$^+$ cells) numbers detected by flow cytometry in the nonhematopoietic of gastric muscles of *klotho* mice (n = 5–6/group). Statistical significance was determined using Kruskal-Wallis 1-way analysis of variance (on ranks). *$P < .05$, **$P < .01$, ***$P < .001$, ****$P < .0001$. ns, not significant.

twice a day for 3 weeks). Gastric KIT protein was reduced in vehicle-treated *klotho* mice and 3-week treatment with EPZ6438 attenuated reduction in gastric KIT and SCF protein in *klotho* mice (Figure 4*A*). EPZ6438 prevented the TRP53-induced increase in H3K27me3 and without affecting TRP53, EZH2 protein expression, and TRP53 phosphorylation by WB (Figure 4*A*). To verify the KIT protein results obtained by immunoblotting, ICC networks were assessed by KIT and ANO1 immunostaining and confocal microscopy. As previously reported,[12] the gastric ICC networks in *klotho* mice were diffusely and uniformly depleted throughout the regions and layers of the gastric corpus (Figure 4*B*) and fundus (Figure 4*C*) compared with WT mice. EPZ6438 treatment also restored reduced gastric ICC networks of *klotho* mice (Figure 4*B* and *C*). By SCF WB, the reduction of SCF was observed in *klotho* mice and 3-week treatment with EPZ6438 was able to prevent this reduction in *klotho* mice (Figure 4*A*), suggesting in vivo EZH2 inhibition also can also mitigate age-related SCF protein reduction. To confirm our WB and immunohistochemistry results, we quantified KIT$^+$CD34$^-$ ICC and KIT^{low}CD34$^+$ ICC-SC within the hematopoietic lineage-negative fraction of the whole gastric tunica muscularis in these mice by using flow cytometry and previously established and validated

protocols.[25,30,33,34] Treatment with EPZ6438 significantly limited the reduction in both ICC and ICC-SC in *klotho* mice (Figure 4*D*).

EPZ6438 Mitigates Aging-associated Decline in Slow Wave Activity and Inhibitory Junction Potentials in Progeric klotho *Mice*

As previously reported by our group,[12] intracellular electrophysiology revealed significantly diminished slow wave amplitudes in the corpus and antrum of *klotho* mice compared with age-matched WT mice (Figure 5*A* and Table 1). Treatment with EPZ6438 restored the reduced slow wave amplitudes in the corpus and antrum of *klotho* mice (Figure 5*A* and Table 2), suggesting a restoration of slow wave activity through the preserved ICC networks in these mice. Previously, we also reported reduced inhibitory junction potentials[12] in the proximal stomach (fundus) in response to electrical stimulation and reduced ex vivo gastric compliance in *klotho* mice.[12] Consistent with these findings, in the current study we also observed reduced fundal inhibitory junction potentials in *klotho* mice, which was significantly improved following EPZ6438 treatment (Figure 5*C*). This finding indicates that preserving ICC with EPZ6438 treatment may enhance the stomach's ability to relax in response to food and to process the ingested contents.

EPZ6438 Improves Impaired Body Weight Gain and Food Intake in Progeric klotho *Mice*

Our previous work suggests that gastric motor dysfunction because of ICC loss contribute to reduced food intake and impaired body weight gain in *klotho* mice.[12,13] Therefore, we also monitored body weight and food intake in mice treated with EPZ6438. Indeed, reduced food intake

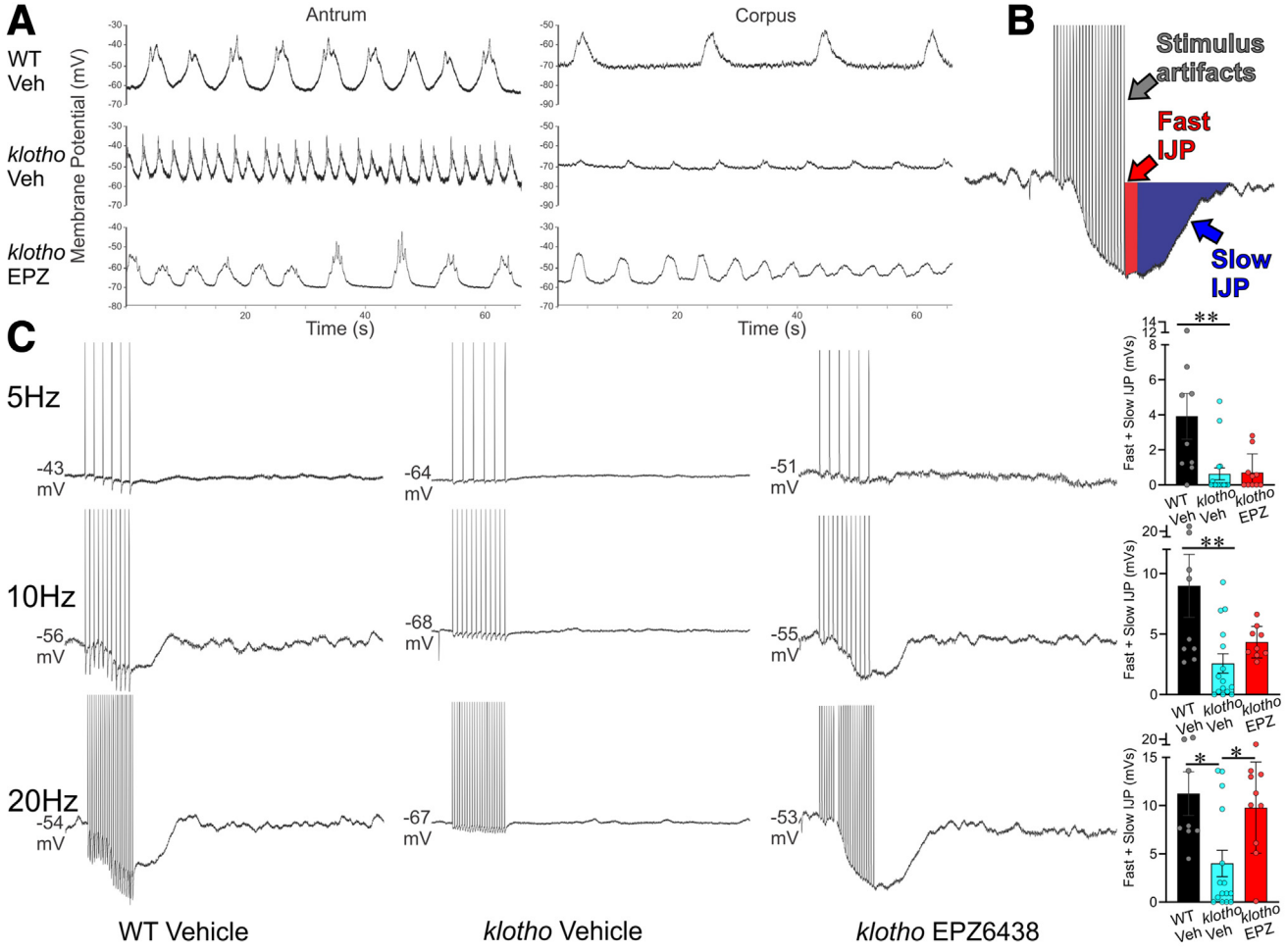

Figure 5. EPZ6438 treatment partially restores reduced slow wave amplitudes and inhibitory neuromuscular transmission in *klotho* mice. (*A*) Representative traces show diminished slow wave amplitudes in the corpus and antrum of *klotho* mice relative to WT control animals. EPZ6438 treatment led to partial restoration of these amplitudes in *klotho* mice. (*B*) Illustration of separation of fast and slow inhibitory junction potentials (IJPs). (*C*) Representative recordings of electrical responses to electrical field stimulation (square pulses delivered by parallel platinum electrodes; 0.3 ms; 5–20 Hz for 1 second; supramaximal voltage). EPZ6438 treatment led to partial restoration of fast and slow IJPs in *klotho* mice. Quantitative analysis of fast and slow IJPs and excitatory junction potentials is shown in Table 1. Statistical significance was determined using Kruskal-Wallis 1-way analysis of variance (on ranks). *$P < .05$, **$P < .01$.

Table 1. Parameters of Postjunctional Electrical Responses to EFS in WT, Veh-Treated *klotho* Mice, and EPZ-treated *klotho* Mice

EFS frequency	Parameter	WT Veh		*klotho* Veh		*klotho* EPZ		*P* (WT Veh vs *klotho* Veh)	*P* (WT Veh vs *klotho* EPZ)	*P* (*klotho* veh vs *klotho* EPZ)
5 Hz	Fast IJP	2.214 ± 0.6908	[0.5573; 1.510; 3.939] (9)	0.2890 ± 0.1692	[0.000; 0.000; 0.2654] (16)	0.3230 ± 0.1328	[0.000; 0.09462; 0.7452] (10)	.001	.0033	.9971
	Slow IJP	0.9944 ± 0.3020	[0.3431; 0.8320; 1.937] (8)	0.3828 ± 0.1998	[0.000; 0.000; 0.5364] (16)	0.3856 ± 0.2173	[0.000; 0.000; 0.7044] (10)	.1839	.2436	> .9999
	Fast + slow IJP	3.919 ± 1.305	[1.113; 2.349; 5.971] (9)	0.6323 ± 0.3415	[0.000; 0.000; 0.6194] (17)	0.7087 ± 0.3354	[0.000; 0.2506; 1.155] (10)	.0031	.0099	.9959
10 Hz	Fast IJP	5.227 ± 1.564	[1.749; 2.836; 9.272] (9)	1.375 ± 0.4402	[0.04487; 0.7626; 2.098] (16)	2.193 ± 0.5199	[1.199; 1.702; 2.646] (10)	.0061	.0596	.7472
	Slow IJP	3.763 ± 1.083	[1.050; 2.606; 6.093] (9)	1.456 ± 0.4640	[0.07564; 0.5321; 2.768] (15)	3.239 ± 0.7012	[1.602; 2.789; 4.039] (10)	.0693	.8804	.1725
	Fast + slow IJP	8.990 ± 2.604	[3.351; 4.577; 14.54] (9)	2.580 ± 0.7995	[0.2551; 1.111; 4.958] (15)	4.340 ± 0.4327	[3.356; 3.807; 5.365] (9)	.0068	.0982	.6403
20 Hz	Fast IJP	5.393 ± 1.282	[3.355; 4.720; 6.090] (8)	1.801 ± 0.6435	[0.000; 0.5436; 2.647] (15)	3.860 ± 1.026	[1.047; 3.616; 6.573] (10)	.0284	.5399	.233
	Slow IJP	7.926 ± 2.614	[2.818; 3.843; 12.47] (9)	2.857 ± 4.228	[0.04420; 0.5175; 5.418] (16)	5.932 ± 1.611	[1.205; 5.260; 9.252] (10)	.0895	.7184	.3689
	Fast + slow IJP	11.24 ± 2.259	[7.369; 7.788; 18.38] (8)	4.004 ± 1.369	[0.000; 0.8982; 9.647] (15)	9.792 ± 1.494	[5.857; 10.67; 13.32] (10)	.0128	.8409	.0357

NOTE. Responses to square wave electrical pulses (0.3 ms; 5–20 Hz for 1 second; supramaximal voltage) are expressed as areas under the curve (mV) (ie, the areas segmented by RMP before electrical simulation and the subsequent junction potentials). Data are mean ± and [median + interquartile range] from 3 WT, 6 *klotho* Veh, and 5 *klotho* EPZ. The number of responses that were analyzed are located in parentheses.
EFS, electrical field stimulation; EPZ, EPZ6438; IJP, inhibitory junction potential; Veh, vehicle; WT, wild-type.

Table 2. Parameters of Gastric Slow Waves in WT, Veh-treated *klotho* Mice and EPZ-Treated *klotho* Mice

Region	Parameter	WT Veh	*klotho* Veh	*klotho* EPZ	*P* value (WT Veh vs *klotho* Veh)
Corpus	RMP, *mV*	-55.09 ± 2.397 [-65.17; -54.61; -48.19]	-56.06 ± 2.178 [-62.29;-57.74;-50.01]	-55.06 ± 2.064 [-62.62;-55.3;-47.63]	.9485
	Frequency, *cycles min-1*	7.114 ± 0.8207 [3.511; 7.175; 9.186]	5.797 ± 0.8511 [2.511; 4.729; 7.000]	5.783 ± 0.6468 [3.542; 4.835; 7.275]	.4626
	Amplitude, *mV*	10.43 ± 0.8029 [7.233; 11.04; 13.26]	12.03 ± 1.503 [6.652; 9.555; 14.57]	10.35 ± 0.9979 [6.082; 9.827; 13.980]	.5969
	Peak voltage, *mV*	-44.65 ± 2.163 [-52.50;-45.73;-37.29]	-44.03 ± 1.899 [-51.90; -43.10; -40.47]	-44.71 ± 1.926 [-51.10;-45.80;-39.53]	.9736
Antrum	RMP, *mV*	-53.47 ± 4.565 [-64.54; -54.33; -45.90]	-61.84 ± 4.221 [-69.55; -66.33; -51.29]	-44.79 ± 2.035 [-52.64; -42.27; -36.06]	.2838
	Frequency, *cycles min-1*	6.124 ± 0.8831 [3.853; 5.280; 8.457]	6.342 ± 0.7499 [5.396; 6.881; 7.578]	6.557 ± 0.5425 [5.269; 6.172; 8.993]	.9827
	Amplitude, *mV*	9.892 ± 2.067 [6.493; 7.488; 16.46]	4.910 ± 1.403 [3.062; 3.958; 6.719]	6.7 ± 0.8776 [3.292; 6.229; 10.16]	.0895
	Peak voltage, *mV*	-43.58 ± 3.414 [-52.51; -43.61; -38.41]	-56.93 ± 3.604 [-65.51; -58.04; -48.23]	-38.09 ± 1.895 [-43.74; -39.30; -30.70]	.0197

NOTE. Impalements were obtained from intact corpus + antrum tissue, demarcated using fine copper wire. Data are mean ± standard error of the mean and [interquartile range + median] from WT (corpus: n = 5 and n = 7 recordings; antrum: n = 9 mice and n = 24 recordings), *klotho* (corpus: n = 3 and n = 6 recordings; antrum: n = 10 mice and n = 26 recordings), and *klotho* EPZ (corpus: n = 6 and n = 17 recordings; antrum: n = 9 mice and n = 26 recordings) mice. *P* values were determined using Kruskal-Wallis 1-way analysis of variance (on ranks).
EPZ, EPZ6438; RMP, resting (diastolic) membrane potential; Veh, vehicle; WT, wild-type.

(Figure 6*A*) and impaired body weight gain (Figure 6*B* and *C*) in *klotho* mice were also improved by EPZ6438, suggesting that prevention of ICC loss may also restore gastric function and lead to improvement of body weight gain. Pharmacologic EZH2 inhibition, including with EPZ6438, has been shown to increase insulin secretion,[35] a potent anabolic hormone.[36] To investigate the potential involvement of insulin in the EPZ6438-mediated improvement of body weight gain, we measured serum insulin levels by enzyme-linked immunosorbent assay. As we previously reported,[12] serum insulin levels in *klotho* mice are significantly reduced (Figure 6*D*). This reduction was partially alleviated by treatment with EPZ6438 in *klotho* mice, although this effect did not reach statistical significance (Figure 6*D*). It is therefore unlikely that increased insulin secretion was the main factor in the normalization of body weight gain by EPZ6438 treatment.

We next aimed to mechanistically link EZH2 inhibition to the prevention of aging-associated ICC loss by deleting the *Ezh2* gene in *Kit*-transcribing cells in 18-month-old $Kit^{creERT2/+};Ezh2^{fl/fl}$ mice. $Kit^{creERT2/+};Ezh2^{fl/fl}$ mice received tamoxifen to induce Cre recombination. Vehicle treated $Kit^{creERT2/+};Ezh2^{fl/fl}$ mice were used as control subjects. To account for potential side effects of tamoxifen,[37] tamoxifen-treated $Kit^{creERT2/+};Ezh2^{+/+}$ mice were used as a secondary control. None of the mice expressed any outward phenotype. Two months following the initiation of tamoxifen treatment, the stomachs of the mice were examined. Tamoxifen-mediated EZH2 knockout significantly increased KIT protein (Figure 7*A*) and the density of ICC networks (Figure 7*B*) in the aged $Kit^{creERT2/+};Ezh2^{fl/fl}$ mice. These results suggest that conditional genomic ablation of *Ezh2* in the ICC lineage mitigates the loss of ICC during aging. Treatment of $Kit^{creERT2/+};Ezh2^{+/+}$ mice with tamoxifen showed no significant difference in ICC compared with vehicle-treated $Kit^{creERT2/+};Ezh2^{fl/fl}$ mice, while also not impacting EZH2 and KIT protein expression or H3K27me3 levels (Figure 7*A*). These data indicate that the ICC restoration of $Kit^{creERT2/+};Ezh2^{fl/fl}$ mice following tamoxifen treatment was specific and not a consequence of tamoxifen's side effects.

Discussion

The loss of ICC is the most prominent cellular change observed during gastric aging, whereas neurons and smooth muscles only change minimally.[12,13,23,24,38] Previously we identified overactive TRP53 as a key trigger of ICC/ICC-SC decline with age. In this study, we linked aging-associated overactive TRP53 to EZH2-mediated KIT and SCF repression and found that these changes play an important role in gastric motor dysfunction. That the loss of ICC is key to the observed aging-associated gastric motor dysfunctions is strongly supported by previous studies in *Kit* hypofunctional mutant W/W^{v} mice and SCF-deficient Sl/Sl^{d} mice[39–41] and by experiments that used neutralizing antibodies to deplete gastric ICC. Pharmacologic and siRNA-mediated inhibition or Cre-mediated in vivo genomic inactivation of EZH2 increased KIT protein expression promoting ICC

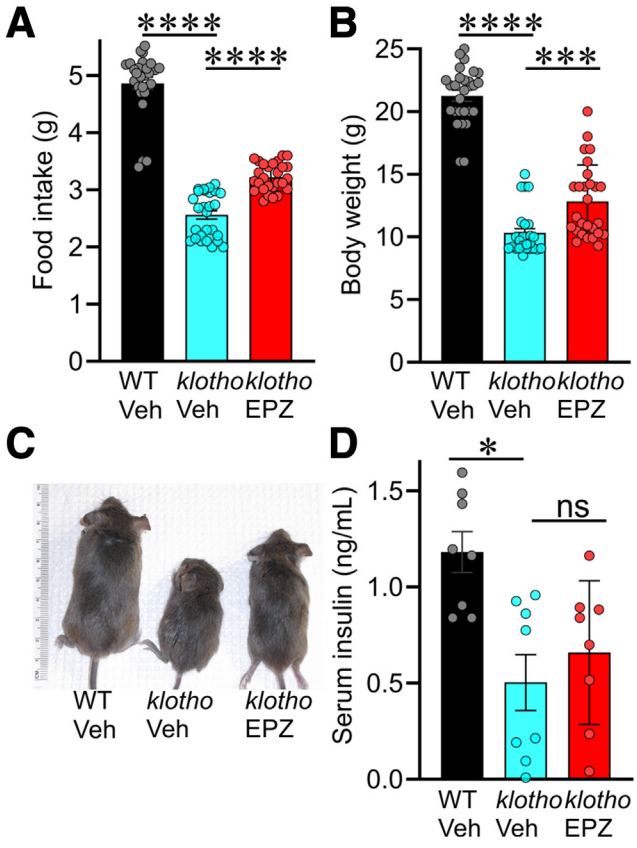

Figure 6. EPZ6438 treatment restored reduced food intake and impaired body weight gain without significantly affecting insulin secretion in *klotho* mice. EPZ6438 treatment restored reduced food intake and impaired body weight gain of *klotho* mice. Restoration of reduced food intake (*A*) and body weight gain (*B* and *C*) of *klotho* mice by EPZ6438 (EPZ) treatment (n = 27/group). (*D*) Reduced serum insulin levels in *klotho* mice were not alleviated by EPZ6438 treatment (n = 8/group). Statistical significance was determined using Kruskal-Wallis 1-way analysis of variance (on ranks). *$P < .05$, ***$P < .001$, ****$P < .0001$. ns, not significant.

preservation and the restoring of slow wave activity and inhibitory junction potentials ex vivo. Based on the foregoing, we suggest that pharmacologic inhibition of EZH2 is a potential pharmacologic approach to restore gastric ICC/ICC-SC depletion and gastric dysfunction with age.

Aging is related to specific changes in histone levels and posttranslational modifications.[42] EZH2 shows an age-related downregulation in senescent human cells and in certain organs, including pancreatic β cells and the liver, in mice.[17,18,38] In contrast, an increase in H3K27me3 levels was observed in skeletal smooth muscles,[43] and decreased levels of H3K27me3 contribute to longer lifespans in *Drosophila*.[44,45] In musculoskeletal tissues and mesenchymal stem cells, EZH2 is elevated in self-renewing stem cells and precursor cells but downregulated during differentiation when cells become quiescent.[46] In this study, we also observed that EZH2 and H3K27me3 levels are elevated in the stomachs of mice and humans with age. Additionally, we found the TRP53 stabilizer nutlin 3a to increase H3K27me3 levels and EZH2 protein in ICC-SC in vitro and in gastric muscles ex vivo. These divergent observations indicate that the important roles of EZH2 in stem cell self-renewal, differentiation, quiescence, and senescence are lineage-specific, providing pharmaceutical opportunities for local tissue-specific intervention.

SCF is widely expressed in stromal tissues and plays critical roles in the development and maintenance of various KIT-expressing cell types, including melanocytes, germinal cells, erythroid lineage cells, mast cells, gastrointestinal stromal tumors, and ICC.[31,32,47,48] Mature ICC maintenance, self-renewal, and differentiation of KIT^{low} ICC-SC depend on SCF production by gastric smooth muscle cells, which form the natural microenvironment for ICC.[29,30] Our recent studies have identified impaired KIT signaling stimulation by low SCF because of aging-related IGF1 decline as one of the key triggers of ICC loss with age.[13] In the present study, we found nutlin 3a-induced TRP53 activation to reduce SCF expression in intact gastric muscles, whereas EPZ6438-mediated EZH2 inhibition alleviated reduced SCF expression in these tissues. Additionally, EPZ6438 treatment also prevented reduced SCF expression in *klotho* mice, confirming our ex vivo findings. Therefore, the protective effect of EPZ6438 on SCF preservation in *klotho* mice may be crucial for ICC maintenance. However, the mechanisms behind the reduction in SCF levels remain unclear and identifying the key signaling cascade mediating reduced SCF expression in gastric tunica muscularis during aging is the next necessary step toward a better understanding of aging-related ICC decline.

Diminished gastric slow wave activity and impaired postjunctional neural responses are key indicators of ICC depletion because of specific genetic mutations, linking ICC loss to gastric motor dysfunction.[40,41,49–51] Reduced fundal relaxation and diminished gastric contractile activity limit the stomach's ability to accommodate and process food and can contribute to early satiety and reduced food intake in elderly individuals.[2,5,52] This association has been experimentally confirmed in both *klotho* and chronologically aged mice.[13,24] Although focal depletion of antral ICC has been linked to delayed gastric emptying of solids in patients and mice with diabetic gastroparesis.[53] Gastric emptying of solids remained unaltered in *klotho* mice with diffuse ICC loss,[12] possibly because of the opposing effects of the depletion of antral and fundal ICC, which would delay[54] and accelerate[12] gastric emptying of solids, respectively (summarized in Figure 8). This interpretation is consistent with the variable rates of gastric emptying reported in elderly individuals (discussed in [12]). In this study, we observed that EPZ6438 treatment significantly restored gastric ICC networks and alleviated the decrease in inhibitory postjunctional neural responses in *klotho* mice. Additionally, EPZ6438 treatment also ameliorated the reduced food intake and impaired body weight gain in these mice, suggesting a functional connection between gastric motor function and food intake, as recently reported by our group.[13] However, the relationship between gastric motor dysfunction and organismal aging is not yet fully understood, indicating the need for further experimental investigation.

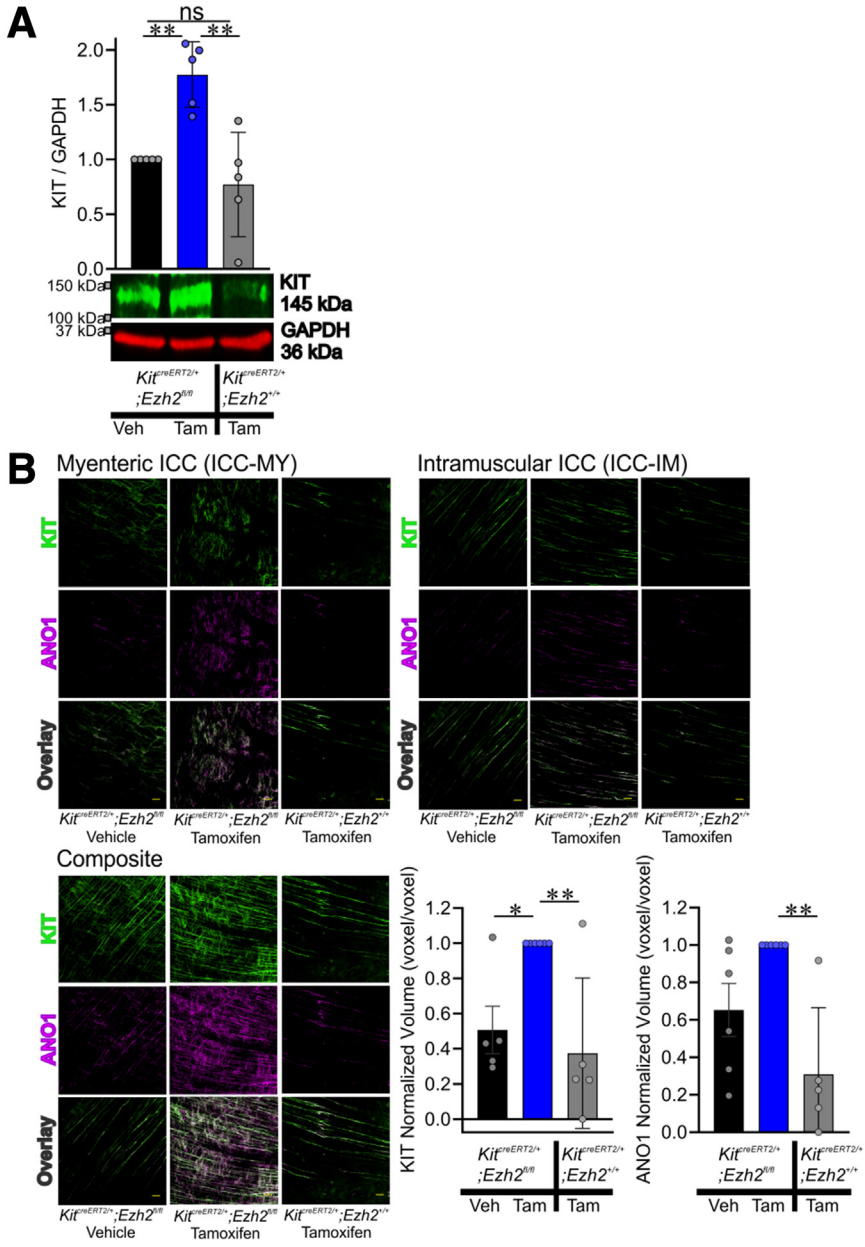

Figure 7. Genomic deletion of Ezh2 in Kit-positive ICC lineage preserved ICC of *Kit*$^{creERT2/+}$;*Ezh2*$^{fl/fl}$ mice with age. (*A*) Tamoxifen (Tam; 0.075 mg/g intraperitoneally for consecutive 3 days at 18 months of age)-induced recombination restored reduced KIT protein of *Kit*$^{creERT2/+}$;*Ezh2*$^{fl/fl}$ mice compared with vehicle (Veh)-treated control mice. Tam-treated *Kit*$^{creERT2/+}$;*Ezh2*$^{+/+}$ mice were served as alternative control. n = 5/group. (*B*) Reduced gastric ICC networks in *Kit*$^{creERT2/+}$;*Ezh2*$^{fl/fl}$ mice were restored by Tam treatment. Representative confocal stacks showing KIT^{+} (*green*) and ANO1^{+} (*magenta*) myenteric ICC (ICC-MY) and intramuscular ICC (ICC-IM) in corresponding regions of the gastric corpus (greater curvature, full thickness) of a *Kit*$^{creERT2/+}$;*Ezh2*$^{fl/fl}$ and *Kit*$^{creERT2/+}$;*Ezh2*$^{+/+}$ mice. n = 5–6/group. Scale bar: 50 μm. Statistical significance was determined using Kruskal-Wallis 1-way analysis of variance (on ranks). *$P < .05$, **$P < .01$. ns, not significant.

EZH2 inhibitors hold significant promise for future cancer therapies, with multiple inhibitors currently in clinical development.[26] EPZ6438 is a first-in-class EZH2 inhibitor that received approval in the United States for treating patients with relapsed or refractory follicular lymphoma[26] and locally advanced and metastatic epithelioid sarcoma not eligible for complete resection.[27] Additional compelling evidence suggests that EPZ6438 is highly effective against various other cancers (a leading cause of mortality) with minimal side effects,[26,27] and EZH2 inhibition, including EPZ6438 treatment, has been shown to extend the lifespan of *Drosophila*.[44,45] Studies also suggest that EPZ6438 has protective effects against depression, liver fibrosis, and intestinal damage,[55–58] and EZH2 inhibition is effective in bone regeneration including restoration of bone mass accrual in estrogen-deficient mice that provide a model for age-related bone loss (ie, osteoporosis).[59] Collectively, the current findings on EZH2 inhibition are strongly encouraging for further research to explore the potential impact of EPZ6438 in aging and aging-related disorders and diseases.

A strength of our study is the combined use of EPZ6438 and GSK126, and several other methods including siRNA-mediated *Ezh2* knock-down in ICC-SC (in vitro) and genomic deletion of *Ezh2* in Kit-positive ICC lineage of *Kit*$^{creERT2/+}$;*Ezh2*$^{fl/fl}$ mice. One limitation of our study is that it remains unclear whether the biologic effects we observed are specific to EZH2 inhibition by EPZ6438 in gastric ICC/ICC-SC. This necessitates further investigation to establish mechanistic links between the cell-, tissue-, and organ-level actions of EZH2 inhibition found in the current set of experiments. Therefore, further in-depth studies need to focus on the stem cells and lineage-specific effects of EZH2 and

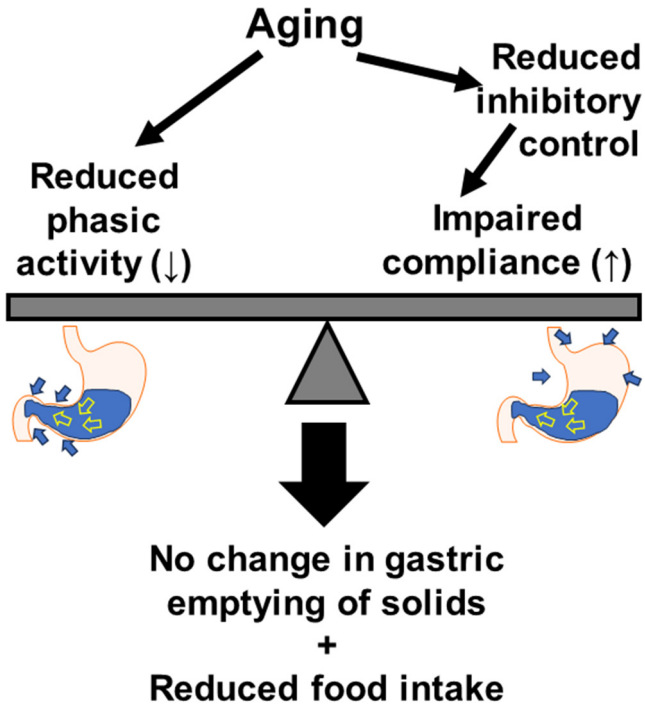

Figure 8. Proposed mechanisms regulating gastric emptying of solids and food intake during aging. Loss of ICC with aging is associated with diminished phasic activity (reduced slow wave amplitudes) and decreased inhibitory (nitrergic) control over smooth muscle relaxation, resulting in impaired compliance. Having opposite effects on gastric emptying, these 2 processes cancel out each other's effects on gastric emptying, while together restricting gastric functions, leading to reduced food intake.

how to generate tissue-exclusive effects that do not impair EZH2 functions in other cells and tissues.

In summary, we found that age-related ICC-SC/ICC decline can be countered by stimulating the SCF-KIT signaling pathway by EZH2 inhibition. The effects of in vivo EPZ6438 are supported by ex vivo (organotypic culture) findings, which demonstrate that EPZ6438 mitigates TRP53 stabilization-induced ICC depletion by activating the SCF-KIT signaling pathway. The prevention of ICC loss by EPZ6438 leads to the recovery of impaired slow wave activity, reduced food intake, and body weight gain in *klotho* mice. These results identify potential pharmacologic targets for therapeutic approaches aimed at restoring gastric motor function, which declines with age.

Materials and Methods

Ethics Statement

Deidentified normal gastric corpus tissues were obtained from patients without diabetes between the ages of 28 and 68 years who were undergoing bariatric surgery for medically complicated obesity (Institutional Review Board protocol 20-012002). These tissues have not been previously studied or reported. Animal experiments were conducted with the guidelines outlined in the National Institutes of Health Guide for the Care and Use of Laboratory Animals. The protocols were approved by the Mayo Clinic Institutional Animal Care and Use Committee (A48315).

Human Tissue Preparation

Full-thickness gastric tissues were obtained from male and female patients. Pieces of gastric tunica muscularis were prepared by cutting away the mucosa and submucosa following the previously described method used for mouse tissues.[30] Subsequently, pieces of gastric tunica muscularis were promptly frozen in liquid nitrogen on removal. Consent was secured and documented in the patients' electronic medical records. None of the patient samples have been used in previous studies.

Animals

Homozygous *klotho* mice hypomorphic for α-Klotho and age-matched WT littermates (both sexes) were obtained from our heterozygous breeders and their genotype verified by polymerase chain reaction as reported previously.[11] *klotho* mouse breeder is a generous gift of Dr Makoto Kuro-o and Dr Ming-Chang Hu (University of Texas Southwestern Medical Center, Dallas, TX). $Kit^{creERT2/+}$ mice (background: C57BL/6)[60] mice were kindly provided by Dr Dieter Saur (Technical University of Munich, Munich, Germany). Mice with a conditional $Ezh2^{fl/fl}$ allele, specifically targeting the SET domain,[61] were acquired from the Mutant Mouse Regional Resource Center (B6;129P2-*Ezh2*tm1Tara/Mmnc, University of North

Table 3. Antibodies Used for Flow Cytometry Analysis of Cells Freshly Dissociated from Murine Gastric Muscles

Target	Supplier	Host/Source	Clone/ID	Isotype	Label	Final conc. or μg/10^6 cells
CD16/32	eBioscience	Rat mAb	93	IgG2a, λ		1 μg
CD11b	eBioscience	Rat mAb	M1/70	IgG_{2b}, κ	PE-Cy7	0.0312 μg
CD45	eBioscience	Rat mAb	30-F11	IgG_{2b}, κ	PE-Cy7	0.0312 μg
F4/80	eBioscience	Rat mAb	BM8	IgG_{2a}, κ	PE-Cy7	0.0625 μg
CD44	BioLegend	Rat mAb	IM7	IgG_{2b}, κ	APC-Cy7	0.0625 μg
KIT	eBioscience	Rat mAb	ACK2	IgG_{2b}, κ	APC	5 μg/mL
KIT	eBioscience	Rat mAb	2B8	IgG_{2b}, κ	APC	0.25 μg
CD34	eBioscience	Rat mAb	RAM34	IgG_{2a}, κ	eFluor 450 or FITC	0.2 μg

FITC, fluorescein isothiocyanate; mAb, monoclonal antibody.

Table 4. Configuration of the Becton Dickinson FACSMelody Cell Sorter

Laser	Detector	Dichroic	Filter
405 nm	C	448/45	Blank
488 nm	A	752 LP	783/56
640 nm	B	660/10	660/10

NOTE. Dichroic mirror (LP, long-pass) and bandpass (center of transmittance/bandwidth) filter data are in nm.

Carolina, Chapel Hill, NC). $Kit^{creERT2/+};Ezh2^{fl/fl}$ mice were generated in our breeding program.

For gastric protein expression by WB, experiments with *klotho* mice were performed between 60 and 70 days of age. C57BL/6 mice 22–24 months old and 8–10 weeks old were from the Jackson Laboratory (Bar Harbor, ME). Mice were sacrificed by CO_2 inhalation anesthesia or by decapitation performed under deep isoflurane (Baxter Healthcare) inhalation anesthesia. Gastric corpus + antrum muscles were prepared as previously described.[32] None of the mice have been used in previous studies.

Animal Experiments

Sex, age, genetic background, and numbers of animals, as well as methods of euthanasia are specified in the main text. None of the mice were used in any previous experiments. Mice were housed a maximum 5 per cage using an Allentown, Inc (Allentown, NJ) reusable static caging system in the Mayo Clinic Department of Comparative Medicine Guggenheim Vivarium under a 12 hour light/12 hour dark cycle. Bedding material was irradiated one-quarter-inch corn cob with the addition of Bed-r'Nest (4 g; The Andersons, Inc, Maumee, OH) irradiated paper-twist nesting material as enrichment. Mice were kept on irradiated PicoLab 5058 Mouse Diet 20 (≥20% protein, ≥9% fat, ≤4% fiber, ≤6.5% ash, ≤12% moisture; LabDiet, Inc, St. Louis, MO). Food and water were available ad libitum.

Induction of Cre-mediated Recombination In Vivo

Cre-mediated recombination was induced with tamoxifen (Sigma-Aldrich, St. Louis, MO) injected intraperitoneally once daily for 3 consecutive days at a dose of 0.075 mg/g body weight in peanut oil vehicle (Sigma Aldrich) containing 10% ethanol (3.75 μL/g body weight) as described previously.[62] $Kit^{creERT2/+};Ezh2^{fl/fl}$ mice underwent tamoxifen treatment when they were 18 months old. Age- and sex-matched $Kit^{creERT2/+};Ezh2^{fl/fl}$ mice were treated with vehicle only as a control. As alternative control to exclude the toxic effect of tamoxifen, age- and sex-matched $Kit^{creERT2/+};Ezh2^{+/+}$ mice were treated with tamoxifen solution.

Table 5. Antibodies Used in WB Studies

Target	Supplier	Host	Clone/ID	Isotype/lot #	Label	Final conc.
ANO1	Abcam (Cambridge, MA)	Rabbit pAb	Ab53212	IgG/GR3295356-1		1:1000
EZH2	CST (Beverly, MA)	Mouse mAb	3147	IgG/4		
GAPDH	Novus	Goat pc	IMG-3073	C3G2		0.05 μg/mL
GAPDH	Sigma	Rabbit pAb	G9545	IgG_1/099M4801V		1:40000
KIT	R&D Systems	Goat pAb	AF1356	IgG/ IEO0217101		0.2 μg/mL for mice
KIT	DAKO (Carpinteria, CA)	Rabbit pAb	A4502	100428020A		1:4000 for human beings
H3K27me3	CST	Rabbit mAb	9733	IgG/8		1:2000
H3	Thermo Fisher	Mouse mc	865R2	IgM/I293050		0.5 μg/mL
SCF	RDS	Goat pAb	AF-455-NA	IgG/AIL0323011		0.1 μg/mL
T-TRP53	CST	Mouse mAb	2524	IgG_1/17		1:2000
P-TRP53 (Ser15)	CST	Rabbit pAb	9284	12		1:1000
Secondary Ab: Anti-rabbit IgG (H + L)	LI-COR	Donkey pAb	#926-32223	C90821-03	IRDye 680	1:10000
Secondary Ab: Anti-mouse IgG (H + L)	LI-COR	Donkey pAb	#926-32222	C71204-03	IRDye 680	1:10000
Secondary Ab: Anti-rabbit IgG (H + L)	LI-COR	Donkey pAb	#926-32213	C70918-03	IRDye 800CW	1:10000
Secondary Ab: Anti-goat IgG (H + L)	LI-COR	Donkey pAb	#926-32214	C80207-07	IRDye 800CW	1:10000

Ab, antibody; GAPDH, glyceraldehyde-3-phosphate dehydrogenase; H + L, highly cross-absorbed; mAb, monoclonal antibody; pAb, polyclonal antibody; SCF, stem cell factor; WB, Western immunoblotting.

Table 6. Antibodies Used in Mouse Immunohistochemistry Studies

Target	Supplier	Host	Clone/ID	Isotype/lot #	Label	Final conc.
ANO1	Abcam	Rabbit pAb	ab53212	IgG/GP3295656-1		1:1500
KIT	R&D Systems	Goat pAb	AF1356	IgG/IEO0217101		0.2 μg/mL
Secondary Ab: Anti-rabbit IgG	Life Technologies (Grant island, NY)	Donkey pAb	A31573	2577247	AF647	5 μg/mL
Secondary Ab: Anti-goat IgG	Life Technologies	Donkey pAb	A11055	2411589	AF488	5 μg/mL

Ab, antibody; pAb, polyclonal antibody.

Ex Vivo Physiological Studies

Electrical slow waves and postjunctional responses to electrical field stimulation of enteric nerves in the circular muscle of the distal stomach (corpus + antrum) and the fundus, respectively, were recorded by an intracellular sharp electrode technique.[30,53,63]

EPZ6438 Treatment

EPZ6438 was obtained from Xcessbio Biosciences, Inc (San Diego, CA), formulated in vehicle (phosphate-buffered saline with 5% dimethyl sulfoxide + 40% PEG300 + 5% Tween80). *klotho* mice received twice daily intraperitoneal injections of EPZ-6438 (160 mg/kg twice a day)[64] for 3 weeks. The same

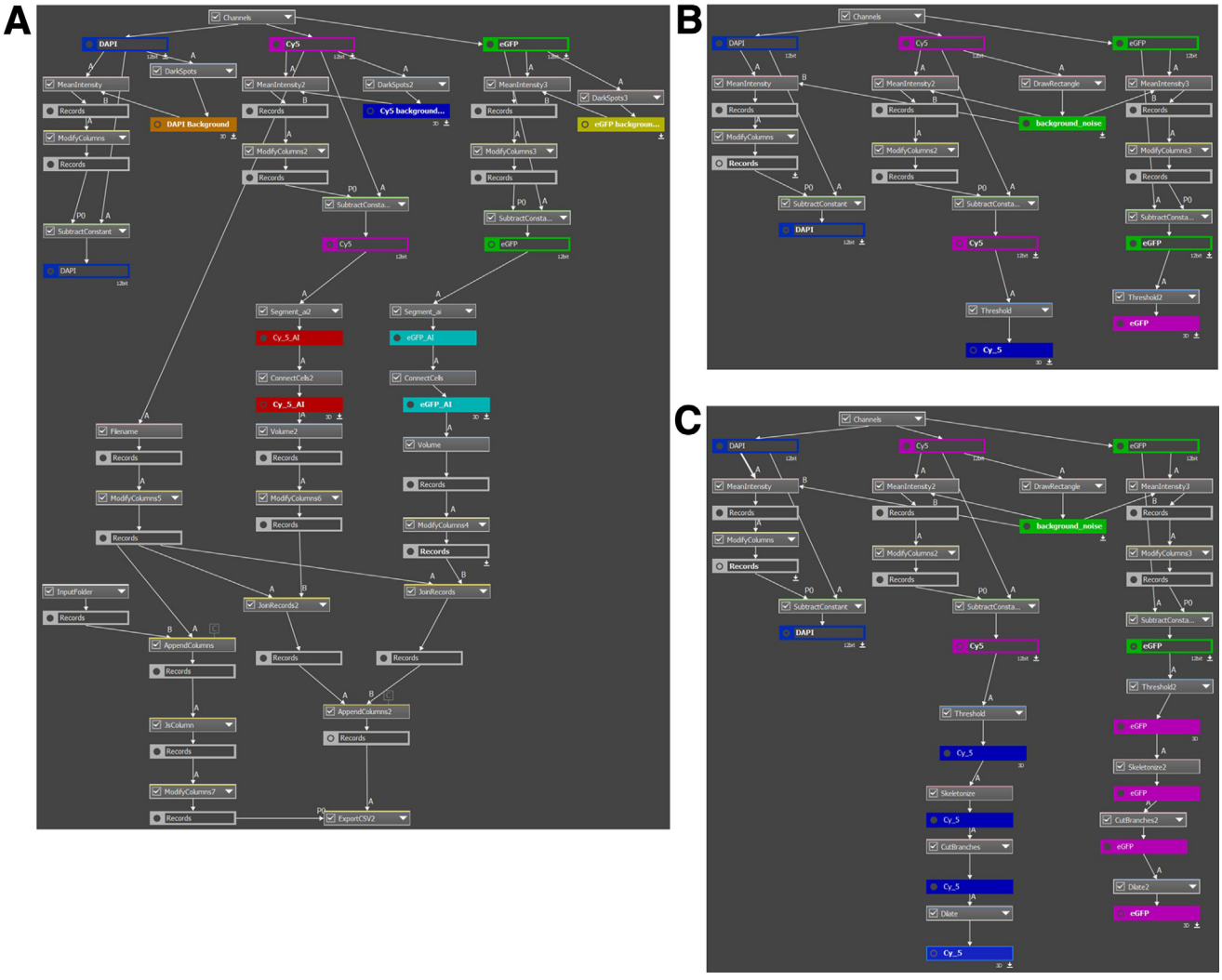

Figure 9. Quantitative image analysis workflow diagrams. (*A*) GA3 recipe for setting background removal, AI-based segmentation, volume quantification, and export. (*B*) GA3 recipe for obtaining the volumes of KIT (enhanced green fluorescent protein; eGFP) or ANO1 (cyanine 5; Cy5) within the flattened segmented areas of KIT (eGFP) or ANO1-positive intramuscular ICC (ICC-IM), which are used for AI training. (*C*) GA3 recipe for obtaining the volumes of KIT (eGFP) or ANO1 (Cy5) within flattened segmented areas of KIT (eGFP) or ANO1-positive myenteric ICC (ICC-MY) that are used for AI training.

Table 7. Software Used in this Study

Software	Source	Identifier
GraphPad Prism 10.1.1	GraphPad Software	https://www.graphpad.com/
Flow Jo 10	BD	https://www.flowjo.com/
Microsoft Excel	Microsoft	https://www.microsoft.com/en-us/microsoft-365/excel
Image Studio	LI-COR	https://www.licor.com/bio/image-studio/
pCLAMP (ClampFit) 11	Molecular Devices	https://www.moleculardevices.com/products/axon-patch-clamp-system/acquisition-and-analysis-software/pclamp-software-suite
AxoScope 11	Molecular Devices	https://support.moleculardevices.com/s/article/Axon-pCLAMP-11-Electrophysiology-Data-Acquisition-Analysis-Software-Download-Page?_gl=1*i7urzg*none_ga*NjE3NzYxODUwLjE3MTY0MjUwNjM.*none_ga_QKBSQT0P0V*MTcxNjQ3MDc2Ny4yLjEuMTcxNjQ3MDc5My4zNC4wLjA.*_gcl_au*MTkxOTcxMTg3OC4xNzE2NDI1MDYz&_ga=2.18292921.1060408156.1716425063-617761850.1716425063
Gen 5	BioTek	https://www.agilent.com/en/product/microplate-instrumentation/microplate-instrumentation-control-analysis-software/imager-reader-control-analysis-software/biotek-gen5-software-for-detection-1623227
NIS Elements	NIKON	https://www.microscope.healthcare.nikon.com/products/software/nis-elements/nis-elements-advanced-research
NIS-ai	NIKON	https://www.microscope.healthcare.nikon.com/products/software/nis-elements/nis-ai-1

amount of vehicle was injected as a control for EPZ6438 treatment. EPZ6438 or vehicle injections was initiated when the mice were 6–7 weeks old (ie, at the time when *klotho* mice began to display a wide array of premature aging phenotypes), which lead to their death at ∼70 days of age.[11]

Serum Insulin Measurement

Blood samples were collected from the submandibular vascular bundle of WT mice, *klotho* mice treated with a vehicle, and *klotho* mice treated with EPZ6438. Serum insulin was measured by RayBio Mouse Insulin enzyme-linked immunosorbent assay kit from RayBiotech (ELM-Insulin; Lot# 032240534, Peachtree Corners, GA).

ICC Stem Cell Line

Isolation and maintenance of the murine ICC-SC cell lines D2211B were previously described by us.[25] Only cells with diploid DNA content and lacking expression of the temperature-sensitive, tsA58-mutant SV40 large T antigen (tsTAg) were used.[25] In this study, D2211B cells were cultured with Medium 199 with phenol red supplemented with 1% antibiotic-antimycotic, 1% L-glutamine (Thermo Fisher Scientific) and 10% fetal bovine serum (Mediatech, Inc, Woodland, CA).

Cell Cultures and EZH2 Inhibitors

To examine the effects of EZH2 inhibition on the growth arrest of ICC-SC induced by nutlin 3a,[13,24] D2211B cells were treated with 30 μmol/L nutlin 3a in combination with EZH2 inhibitors (EPZ6438 and GSK126). Medium containing these compounds were changed every day for 3 days.

RNA Interference

Ezh2 knockdown was performed using Dhamacon ON-TARGETplus SMARTpool siRNA or corresponding Scr (25 nM) and DharmaFECT1 Transfection Reagent (Thermo Fisher Scientific, Waltham, MA) according to the manufacturer's protocol. Treatment was applied following 1-day culturing in antibiotic- and antimycotic-free media. Knockdown efficacy was assessed after 72 hours by WB.

Assay of Cell Viability of ICC-SC

Three thousand cells per well were plated in complete media in 96-well flat-bottom plates. After 72 hours, cells were incubated as indicated. Viable cell counts were evaluated by MTS assay (CellTiter 96 AQueous Non-Radioactive Cell Proliferation Assay, Promega, Madison, WI) according to the manufacturer's protocol.

Multiparameter Flow Cytometry

Murine gastric $KIT^{+}CD44^{+}CD34^{-}$ ICC and $KIT^{low}CD44^{+}CD34^{+}$ ICC-SC were enumerated using previously published and established protocols and reagents (Table 3 for antibodies).[24,25,30,33,34,65] Samples were analyzed by using a Becton Dickinson FACSMelody Cell Sorter (Table 4 for configuration) and FlowJo software (Treestar, Woodburn, OR).

Western Immunoblotting

Tissue and cell lysates were prepared and subjected to sodium dodecyl sulfate-polyacrylamide gel electrophoresis and immunoblotting as described previously[32] (see antibodies in Table 5). Target and reference proteins were detected simultaneously using LI-COR Biosciences (Lincoln, NE) secondary antibodies tagged with near-infrared and infrared fluorescent dyes (IRDye700: red

pseudocolor; IRDye800CW: green pseudocolor). Blots were visualized using an Odyssey XF Imaging System (LI-COR Bioscience) and quantified using LI-COR Image Studio version 5.0. Protein bands of interest were expressed in densitometric units normalized to the loading control (glyceraldehyde-3-phosphate dehydrogenase) detected simultaneously in the same sample and in the same blots. Quantitative comparisons of loading control-normalized data were made between samples acquired and processed independently.

Immunohistochemistry and Confocal Microscopy

Whole-mount of freshly dissected intact gastric tunica muscularis tissues were processed using established techniques.[29] Briefly, tissues were fixed with methanol (30 minutes) and blocked with 1% bovine serum albumin (Sigma-Aldrich). ICC were detected with goat polyclonal anti-murine KIT antibodies and rabbit polyclonal anti-ANO1 antibodies (72 hours at 4°C; see Table 6 for detailed antibody information). Bound antibodies were detected with alexa fluor (AF) 488 donkey anti-goat and AF647 donkey anti-rabbit IgG (24 hours at 4°C; see Table 6 for detailed antibody information). Nuclei were counterstained with 4′,6-diamidino-2-phenylindole (DAPI, Thermo Fisher; 1:600) at room temperature for 30 minutes. Whole-mount images were acquired with a Nikon (Nikon Corporation, Minato City, Japan) AX R confocal system coupled to a Nikon Ti2-E inverted microscope using a Nikon Plan Apo λ 20x lens. The AX R has 8 laser lines (405, 445, 488, 514, 561, 594, 640, and 730 nm) in 2 launches for excitation, a 2k pps resonant and an 8k pps Galvano scan head with 5 detectors including DUX-VB4 detector for NIR, 2 tunable and 1 filter-based GaAsP detectors, and 1 filter-based high-sensitivity PMT capable of 25-mm fields-of-view. DAPI, AF488, and AF647 were excited with the 405-nm, 488-nm, and 640-nm laser lines, respectively (DM: DM405/488/561/640) and detected with the following emission filters: 430–475 nm, 499–551 nm, and 663–738 nm, respectively. Z-stack images of immunostained gastric ICC were captured with NIS-Elements AR 5.41.00 software at a resolution of 295 $\times$ 295 $\times$ 0.47 μm per pixel using a pinhole size of 0.9 AU at 640 nm.

For quantitative image analysis, the acquired images were processed using Nikon's NIS-Elements Segmentation AI (Segment.ai) software, which uses advanced machine learning algorithms for image analysis and segmentation. To delineate regions of interest within the acquired images and extract pixelated/volumetric data, we used GA3 recipes specifically designed for automated segmentation tasks (Figure 9*A*). The segmentation process involved adjusting the algorithm parameters to optimize accuracy and minimize background noise. Segmentation was applied to the flattened confocal stacks using KIT and ANO1 staining for intramuscular ICC (Figure 9*B*) and myenteric ICC (Figure 9*C*). We also trained the Segment.ai software, using these segmentations, to reconstruct the 3-dimensional volume of the KIT^+ and $ANO1^+$ ICC from the confocal stacks. The AI-based GA3 protocols process the inputted images by automatically detecting regions of low fluorescence, averaging an intensity value, and subtracting it from each fluorescence channel to reduce background noise. The images are then processed by our trained Segment.ai software, which automatically detects and segments ICC networks. These networks are connected between the optical sections to create 3-dimensional objects, which are then measured for volume. These values are automatically exported into a separate folder as Excel files for further data analysis. Cumulative volumetric data was then normalized and reported. Manual validation and refinement of the segmented regions were conducted to ensure accuracy and reliability in the AI training process.

Materials

Nutlin 3a and nutlin 3b were from Cayman Chemical (Ann Arbor, MI). Dimethyl sulfoxide, tamoxifen, and Triton-X were from Sigma-Aldrich (St. Louis, MO), PEG300 was from Selleckchem (Houston, TX), and Tween80 and Tween20 was from Bio-Rad laboratories (Hercules, CA). EPZ6438 and GSK126 were from Xcessbio Biosciences, Inc (San Diego, CA). 4',6-diamidino-2-phenylindole (DAPI) and SlowFade Diamond Antifade Mountant were purchased from Thermo Fisher Scientific, Waltham, MA. The software used in this study is listed in Table 7.

Statistical Analyses

Data were expressed as mean $\pm$ standard deviation. Each graph contains an overlaid scatter plot showing all independent observations. The "n" in the figure legends refers to these independent observations. Statistical significance of survival curves was analyzed with log-rank test. All other statistical analyses were performed by nonparametric methods including the Mann-Whitney rank sum test and the Kruskal-Wallis 1-way analysis of variance on ranks followed by appropriate post hoc tests. A P value less than .05 was considered statistically significant.

References

1. Moqri M, Herzog C, Poganik JR, et al. Biomarkers of aging for the identification and evaluation of longevity interventions. Cell 2023;186:3758–3775.
2. Nguyen VTT, Taheri N, Chandra A, et al. Aging of enteric neuromuscular systems in gastrointestinal tract. Neurogastroenterol Motil 2022;34:e14352.
3. Choi EL, Taheri N, Chandra A, et al. Cellular senescence, inflammation, and cancer in the gastrointestinal tract. Int J Mol Sci 2023;24:9810.
4. Camilleri M, Cowen T, Koch TR. Enteric neurodegeneration in ageing. Neurogastroenterol Motil 2008;20:185–196.
5. Parker BA, Chapman IM. Food intake and ageing: the role of the gut. Mech Ageing Dev 2004;125:859–866.
6. Senior AM, Solon-Biet SM, Cogger VC, et al. Dietary macronutrient content, age-specific mortality and lifespan. Proc Biol Sci 2019;286:20190393.

7. Longo VD, Anderson RM. Nutrition, longevity and disease: from molecular mechanisms to interventions. Cell 2022;185:1455–1470.
8. Morley JE. Anorexia of ageing: a key component in the pathogenesis of both sarcopenia and cachexia. J Cachexia Sarcopenia Muscle 2017; 8:523–526.
9. Sanders KM, Santana LF, Baker SA. Interstitial cells of Cajal: pacemakers of the gastrointestinal tract. J Physiol Published online November 23, 2023. https://doi.org/10.1113/JP284745.
10. Huizinga JD, Zarate N, Farrugia G. Physiology, injury, and recovery of interstitial cells of Cajal: basic and clinical science. Gastroenterology 2009;137:1548–1556.
11. Kuro-o M, Matsumura Y, Aizawa H, et al. Mutation of the mouse klotho gene leads to a syndrome resembling ageing. Nature 1997;390:45–51.
12. Izbeki F, Asuzu DT, Lorincz A, et al. Loss of Kitlow progenitors, reduced stem cell factor and high oxidative stress underlie gastric dysfunction in progeric mice. J Physiol 2010;588:3101–3117.
13. Truong Thuy Nguyen V, Taheri N, Choi EL, et al. Insulin-like growth factor 1 preserves gastric pacemaker cells and motor function in aging via ERK1/2 activation. Cell Mol Gastroenterol Hepatol 2023;16:369–383.
14. Young K, Eudy E, Bell R, et al. Decline in IGF1 in the bone marrow microenvironment initiates hematopoietic stem cell aging. Cell Stem Cell 2021;28:1473–1482.e7.
15. Cao R, Wang L, Wang H, et al. Role of histone H3 lysine 27 methylation in Polycomb-group silencing. Science 2002;298:1039–1043.
16. Kim JJ, Kingston RE. Context-specific Polycomb mechanisms in development. Nat Rev Genet 2022; 23:680–695.
17. Bracken AP, Dietrich N, Pasini D, et al. Genome-wide mapping of Polycomb target genes unravels their roles in cell fate transitions. Genes Dev 2006;20:1123–1136.
18. Chen H, Gu X, Su IH, et al. Polycomb protein Ezh2 regulates pancreatic beta-cell Ink4a/Arf expression and regeneration in diabetes mellitus. Genes Dev 2009; 23:975–985.
19. Feser J, Tyler J. Chromatin structure as a mediator of aging. FEBS Lett 2011;585:2041–2048.
20. Noer A, Lindeman LC, Collas P. Histone H3 modifications associated with differentiation and long-term culture of mesenchymal adipose stem cells. Stem Cells Dev 2009;18:725–736.
21. Zhou JX, Dhawan S, Fu H, et al. Combined modulation of polycomb and trithorax genes rejuvenates beta cell replication. J Clin Invest 2013;123:4849–4858.
22. SanMiguel JM, Young K, Trowbridge JJ. Hand in hand: intrinsic and extrinsic drivers of aging and clonal hematopoiesis. Exp Hematol 2020;91:1–9.
23. Kwon YH, Kim N, Nam RH, et al. Change in the interstitial cells of Cajal and nNOS positive neuronal cells with aging in the stomach of F344 rats. PLoS One 2017;12: e0169113.
24. Hayashi Y, Asuzu DT, Bardsley MR, et al. Wnt-induced, TRP53-mediated cell cycle arrest of precursors underlies interstitial cell of Cajal depletion during aging. Cell Mol Gastroenterol Hepatol 2021;11:117–145.
25. Bardsley MR, Horvath VJ, Asuzu DT, et al. Kitlow stem cells cause resistance to Kit/platelet-derived growth factor alpha inhibitors in murine gastrointestinal stromal tumors. Gastroenterology 2010;139:942–952.
26. Kim KH, Roberts CW. Targeting EZH2 in cancer. Nat Med 2016;22:128–134.
27. Hoy SM. Tazemetostat: first approval. Drugs 2020; 80:513–521.
28. Harding T, Swanson J, Van Ness B. EZH2 inhibitors sensitize myeloma cell lines to panobinostat resulting in unique combinatorial transcriptomic changes. Oncotarget 2018;9:21930–21942.
29. Horvath VJ, Vittal H, Lorincz A, et al. Reduced stem cell factor links smooth myopathy and loss of interstitial cells of Cajal in murine diabetic gastroparesis. Gastroenterology 2006;130:759–770.
30. Lorincz A, Redelman D, Horvath VJ, et al. Progenitors of interstitial cells of Cajal in the postnatal murine stomach. Gastroenterology 2008;134:1083–1093.
31. Tieniber AD, Rossi F, Hanna AN, et al. Multiple intratumoral sources of kit ligand promote gastrointestinal stromal tumor. Oncogene 2023;42:2578–2588.
32. Hayashi Y, Asuzu DT, Gibbons SJ, et al. Membrane-to-nucleus signaling links insulin-like growth factor-1- and stem cell factor-activated pathways. PLoS One 2013;8: e76822.
33. Wang Y, Marino-Enriquez A, Bennett RR, et al. Dystrophin is a tumor suppressor in human cancers with myogenic programs. Nat Genet 2014;46:601–606.
34. Hayashi Y, Bardsley MR, Toyomasu Y, et al. Platelet-derived growth factor receptor-alpha regulates proliferation of gastrointestinal stromal tumor cells with mutations in KIT by stabilizing ETV1. Gastroenterology 2015; 149:420–432.e16.
35. Al-Hasani K, Marikar SN, Kaipananickal H, et al. EZH2 inhibitors promote beta-like cell regeneration in young and adult type 1 diabetes donors. Signal Transduct Target Ther 2024;9:2.
36. Pessin JE, Saltiel AR. Signaling pathways in insulin action: molecular targets of insulin resistance. J Clin Invest 2000;106:165–169.
37. Xie Z, McGrath C, Sankaran J, et al. Low-dose tamoxifen induces significant bone formation in mice. JBMR Plus 2021;5:e10450.
38. Choi EL, Taheri N, Tan E, et al. The crucial role of the interstitial cells of Cajal in neurointestinal diseases. Biomolecules 2023;13:1358.
39. Fox EA, Phillips RJ, Byerly MS, et al. Selective loss of vagal intramuscular mechanoreceptors in mice mutant for steel factor, the c-Kit receptor ligand. Anat Embryol (Berl) 2002;205:325–342.
40. Burns AJ, Lomax AE, Torihashi S, et al. Interstitial cells of Cajal mediate inhibitory neurotransmission in the stomach. Proc Natl Acad Sci U S A 1996;93:12008–12013.
41. Beckett EA, Horiguchi K, Khoyi M, et al. Loss of enteric motor neurotransmission in the gastric fundus of Sl/Sl(d) mice. J Physiol 2002;543:871–887.

42. Yang JH, Hayano M, Griffin PT, et al. Loss of epigenetic information as a cause of mammalian aging. Cell 2023; 186:305–326.e27.
43. Liu L, Cheung TH, Charville GW, et al. Chromatin modifications as determinants of muscle stem cell quiescence and chronological aging. Cell Rep 2013;4:189–204.
44. Siebold AP, Banerjee R, Tie F, et al. Polycomb repressive complex 2 and trithorax modulate Drosophila longevity and stress resistance. Proc Natl Acad Sci U S A 2010; 107:169–174.
45. Xia B, de Belle JS. Transgenerational programming of longevity and reproduction by post-eclosion dietary manipulation in Drosophila. Aging (Albany NY) 2016; 8:1115–1134.
46. Dudakovic A, Camilleri ET, Paradise CR, et al. Enhancer of zeste homolog 2 (Ezh2) controls bone formation and cell cycle progression during osteogenesis in mice. J Biol Chem 2018;293:12894–12907.
47. Lennartsson J, Ronnstrand L. Stem cell factor receptor/c-Kit: from basic science to clinical implications. Physiol Rev 2012;92:1619–1649.
48. Sanders KM, Ward SM. Kit mutants and gastrointestinal physiology. J Physiol 2007;578:33–42.
49. Sung TS, Hwang SJ, Koh SD, et al. The cells and conductance mediating cholinergic neurotransmission in the murine proximal stomach. J Physiol 2018; 596:1549–1574.
50. Gibbons SJ. Not just there to fill space: profound observations on interstitial cells of Cajal in the gastric fundus. J Physiol 2018;596:1535–1536.
51. Dickens EJ, Edwards FR, Hirst GD. Selective knockout of intramuscular interstitial cells reveals their role in the generation of slow waves in mouse stomach. J Physiol 2001;531:827–833.
52. Bhutto A, Morley JE. The clinical significance of gastrointestinal changes with aging. Curr Opin Clin Nutr Metab Care 2008;11:651–660.
53. Ordog T, Takayama I, Cheung WK, et al. Remodeling of networks of interstitial cells of Cajal in a murine model of diabetic gastroparesis. Diabetes 2000;49:1731–1739.
54. Grover M, Farrugia G, Lurken MS, et al. Cellular changes in diabetic and idiopathic gastroparesis. Gastroenterology 2011;140:1575–1585.e8.
55. Carrasco ME, Thaler R, Nardocci G, et al. Inhibition of Ezh2 redistributes bivalent domains within transcriptional regulators associated with WNT and Hedgehog pathways in osteoblasts. J Biol Chem 2023;299:105155.
56. Wang W, Qin X, Wang R, et al. EZH2 is involved in vulnerability to neuroinflammation and depression-like behaviors induced by chronic stress in different aged mice. J Affect Disord 2020;272:452–464.
57. Qu M, Xiong L, Lyu Y, et al. Establishment of intestinal organoid cultures modeling injury-associated epithelial regeneration. Cell Res 2021;31:259–271.
58. Song P, Duan JL, Ding J, et al. Cellular senescence primes liver fibrosis regression through Notch-EZH2. MedComm (2020) 2023;4:e346.
59. Dudakovic A, Camilleri ET, Riester SM, et al. Enhancer of Zeste Homolog 2 inhibition stimulates bone formation and mitigates bone loss caused by ovariectomy in skeletally mature mice. J Biol Chem 2016; 291:24594–24606.
60. Klein S, Seidler B, Kettenberger A, et al. Interstitial cells of Cajal integrate excitatory and inhibitory neurotransmission with intestinal slow-wave activity. Nat Commun 2013;4:1630.
61. Su IH, Basavaraj A, Krutchinsky AN, et al. Ezh2 controls B cell development through histone H3 methylation and Igh rearrangement. Nat Immunol 2003;4:124–131.
62. Gao F, Hayashi Y, Saravanaperumal SA, et al. Hypoxia-inducible factor 1alpha stabilization restores epigenetic control of nitric oxide synthase 1 expression and reverses gastroparesis in female diabetic mice. Gastroenterology 2023;165:1458–1474.
63. Ordog T, Ward SM, Sanders KM. Interstitial cells of Cajal generate electrical slow waves in the murine stomach. J Physiol 1999;518:257–269.
64. Knutson SK, Kawano S, Minoshima Y, et al. Selective inhibition of EZH2 by EPZ-6438 leads to potent antitumor activity in EZH2-mutant non-Hodgkin lymphoma. Mol Cancer Ther 2014;13:842–854.
65. Hayashi Y, Toyomasu Y, Saravanaperumal SA, et al. Hyperglycemia increases interstitial cells of Cajal via MAPK1 and MAPK3 signaling to ETV1 and KIT, leading to rapid gastric emptying. Gastroenterology 2017; 153:521–535.e20.

Received January 24, 2024. Accepted June 27, 2024.

Correspondence
Address correspondence to: Yujiro Hayashi, PhD, Mayo Clinic, Guggenheim 10-11A, 200 1st Street SW, Rochester, Minnesota 55905. e-mail: hayashi.yujiro@mayo.edu.

Acknowledgements
The image in Figure 8 was produced using MOTIFOLIO.

CRediT Authorship Contributions
Negar Taheri, MD (Formal analysis: Equal; Investigation: Equal; Validation: Equal)
Egan L. Choi (Formal analysis: Equal; Investigation: Equal; Writing – review & editing: Supporting)
Vy Truong Thuy Nguyen (Investigation: Supporting)
Yuebo Zhang (Investigation: Supporting)
Nick M. Huynh (Investigation: Supporting)
Todd A. Kellogg, MD (Resources: Supporting)
Andre J. van Wijnen, PhD (Conceptualization: Supporting; Resources: Supporting; Writing – review & editing: Supporting)
Tamas Ordog, MD (Conceptualization: Supporting; Formal analysis: Supporting; Methodology: Supporting; Supervision: Supporting; Writing – review & editing: Equal)
Yujiro Hayashi, PhD (Conceptualization: Lead; Formal analysis: Lead; Investigation: Equal; Methodology: Lead; Supervision: Lead; Writing – original draft: Lead; Writing – review & editing: Lead)

Conflicts of interest
The authors disclose no conflicts.

Funding
This work was supported in part by National Institutes of Health grants R01 DK121766 (Y.H.), P30 DK084567 (Mayo Clinic Center for Cell Signaling in Gastroenterology), a Mayo Clinic Center for Biomedical Discovery Pilot Award (Y.H.), and an American Gastroenterology Association-Allergan Foundation Pilot Research Award in Gastroparesis (Y.H.). Key resources used in this study were developed with support from R01 DK058185 (T.O.). The funding agencies had no role in the study analysis or writing of the manuscript. The contents of this manuscript are solely the responsibility of the authors.